

# Bound Trions in Two-Dimensional Monolayers: A Review

Roman Ya. Kezerashvili

*New York City College of Technology, The City University of New York, Brooklyn, NY, USA  
The Graduate School and University Center, The City University of New York, New York, NY, USA and  
Long Island University, Brooklyn, NY, USA*

(Dated: March 10, 2026)

Trions—Coulomb-bound three-particle excitations composed of two like-charge carriers and one oppositely charged carrier—are central quasiparticles in two-dimensional semiconductors. Reduced dielectric screening and quantum confinement strongly enhance their binding energies, making them robust and experimentally accessible. This review surveys theoretical and experimental advances in trion physics, emphasizing rigorous few-body approaches and the role of dielectric environment, anisotropy, and external electric and magnetic fields. We analyze computational methods for describing trions in two-dimensional configuration spaces and discuss how reduced dimensionality modifies their structure and stability. Connections to many-body phenomena, including screening, Landau-level mixing, and exciton–polaron crossover, are also highlighted.

## I. INTRODUCTION

The conceptual roots of trions lie in the theory of excitons, introduced by Frenkel in 1931 and later refined by Wannier and Mott, who established the framework for Wannier–Mott excitons in semiconductors [1, 2]. An exciton is a bound state of an electron and a hole held together by the Coulomb attraction between their opposite charges. In typical semiconductors, the exciton Bohr radius—associated with the relative motion of the electron and hole—is much larger than the lattice constant. Consequently, excitons in inorganic semiconductors are well described as weakly bound Wannier–Mott excitons [3, 4], in contrast to tightly bound Frenkel excitons characteristic of molecular and organic crystals [5].

The concept of charged excitonic complexes, now commonly referred to as trions, predates the modern era of atomically thin materials by several decades. It emerged naturally from early developments in exciton physics and from the study of Coulomb-bound few-body systems in semiconductors. Once excitons were recognized as elementary quasiparticles in insulating and semiconducting crystals, it became clear that an exciton could, in principle, bind an additional electron or hole, forming a stable three-particle complex.

The first systematic theoretical description of such complexes was provided by Lampert [6] in 1958. He introduced charged excitons as effective-mass analogues of the negative hydrogen ion in solids and demonstrated that an exciton can bind an extra electron or hole, giving rise to negatively charged ( $X^-$ ) or positively charged ( $X^+$ ) excitons. These three-particle bound states were later termed *trions* to emphasize their composite nature. Early theoretical studies treated trions as few-body Coulomb systems within the effective-mass approximation, identifying the carrier effective masses and dielectric screening as key parameters governing their stability and binding energies.

This review presents a comprehensive overview of the few-body physics of trions in reduced-dimensional semiconductors, with particular emphasis on two-dimensional (2D) materials. It is organized as follows.

Sections II and III provide a historical and conceptual overview of trion physics, beginning with the pre-graphene era in bulk and quantum-well semiconductors and progressing toward atomically thin systems.

Section IV discusses charge–charge interactions in 2D monolayers, with emphasis on dielectric screening and reduced-dimensional effects. A systematic summary of experimental observations of trions in 2D monolayers is presented in Section V.

Section VI introduces the general three-body theoretical formalism within the effective-mass framework and reviews major computational and analytical approaches, including variational and stochastic variational methods, exact diagonalization, Gaussian expansion techniques, diffusion and path-integral quantum Monte Carlo methods, Faddeev equations, and the hyperspherical harmonics method.

Section VII benchmarks theoretical approaches against reported trion binding energies in 2D monolayers. Section VIII examines the influence of external electric and magnetic fields on trions in 2D materials, highlights the distinctive role of group-IV monolayers, and discusses magnetotriton dynamics, emphasizing the necessity of exact Landau-level mixing and the intrinsic coupling between center-of-mass and internal degrees of freedom for reliable modeling in magnetic fields. Concluding remarks are presented in Section IX.

## II. OVERVIEW OF TRIONS BEFORE THE GRAPHENE ERA

Lampert's original prediction of charged excitons [6] represents the canonical starting point of virtually all modern discussions of trion physics. During the 1960s and 1970s, subsequent theoretical studies examined excitons bound to impurities and free carriers in bulk semiconductors. In particular, Moskalenko [7], building on the exciton framework summarized by Mott [8], presented one of the earliest microscopic treatments of impurity-bound excitons, analyzing their Coulomb binding to charged centers and their radiative recombination. It was demonstrated that such complexes give rise to distinct luminescence lines shifted relative to free-exciton emission. Although this work focused on impurity-bound states rather than free three-particle complexes, it clearly established that excitons can bind additional charges while remaining optically active, thereby anticipating the concept of charged excitons and providing an early foundation for modern trion theory.

In the late 1970s, extremely weakly bound three-particle Coulomb complexes were observed in bulk semiconductors such as Ge and Si [9–11]. These findings motivated quantitative theoretical descriptions of negative donor ion ( $D^-$ ) states in bulk materials. In particular, Kamimura *et al.* [12] and Chang [13] developed effective-mass-based theories incorporating realistic multivalley band-structure effects for Ge and Si, treating  $D^-$  states as weakly bound three-body Coulomb systems. Together, these works established benchmark descriptions of bulk three-particle binding that informed and guided later studies of trions in reduced-dimensional semiconductor systems.

A rigorous three-body treatment of charged excitonic complexes in bulk semiconductors was presented in Ref. [14] using the Faddeev-equation framework, focusing on the stability of negatively and positively charged trions under realistic effective-mass and dielectric-screening conditions. The study shows that while negatively charged trions,  $X^-$ , may exist as extremely weakly bound states under favorable circumstances, positively charged trions,  $X^+$ , are intrinsically unstable in bulk materials, even when realistic mass ratios and Coulomb interactions are taken into account. This fundamental asymmetry originates from strong dielectric screening, the absence of confinement, and the large effective masses of holes in bulk semiconductors: a positively charged trion, composed of two holes and one electron, exhibits strongly suppressed hole delocalization due to the heavy hole masses, leading to a more compact spatial distribution of the two holes and enhanced direct Coulomb repulsion in the positively charged trion. Therefore, the hole-hole Coulomb repulsion cannot be compensated by electron-mediated attraction. As a result,  $X^+$  complexes are energetically unstable against dissociation, explaining their systematic absence in bulk-semiconductor experiments.

Thus, in three-dimensional materials, strong dielectric screening significantly reduced the trion binding energies, typically to the scale of a few meV or less. As a consequence, experimental identification of trions in bulk systems remained elusive for many years.

Early bulk evidence for extremely weak three-body Coulomb binding in semiconductors (e.g.,  $D^-$  negative-ion analogs in doped Ge/Si) preceded the high-quality heterostructure era. The situation changed substantially in the 1990s with the development of high-quality semiconductor heterostructures and quantum wells. Reduced dimensionality enhances Coulomb interactions and suppresses screening, thereby stabilizing few-body excitonic complexes. Throughout the 1980s, variational and numerical calculations within different theoretical frameworks predicted that trions in quasi-two-dimensional systems should possess experimentally resolvable binding energies [15]. These predictions were spectacularly confirmed in the early 1990s by photoluminescence experiments in GaAs/AlGaAs quantum wells, which provided the first unambiguous observation of negatively charged excitons [16]. In the 1990s, high-quality semiconductor quantum wells allowed precise studies of trion states using optical measurements [16–19]. Subsequent experiments identified both  $X^-$  and  $X^+$  states and clarified their spin structure, optical selection rules, and magnetic-field dependence [20].

By the late 1990s and early 2000s, trions had become a well-established element of semiconductor many-body physics. An analytically guided variational/adiabatic framework was developed for indirect trions in double quantum wells [21], demonstrating that interwell separation introduces a critical distance beyond which the trion becomes unbound. This framework provides practical scaling trends and estimates for GaAs- and ZnSe-based heterostructures. The binding mechanism is physically transparent: the electron mediates an effective attraction between the two holes, which persists only up to a tunable layer separation. Advanced theoretical approaches, including the method of hyperspherical harmonics [22], configuration interaction method [23], exact diagonalization [24] method, and quantum Monte Carlo simulations [25], were employed to compute trion binding energies and wave functions with high accuracy [26]. Experimental studies have been extended to a variety of material systems, such as CdTe- and ZnSe-based quantum wells, and have explored regimes of strong magnetic fields, where trions coexist and interact with fractional quantum Hall states [27].

To summarize, negatively,  $X^-$ , and positively,  $X^+$ , charged trions confined in quantum wells, and subjected to external magnetic or electric fields, have been the subject of extensive experimental [17–19, 28–38] and theoretical [15, 26, 32, 39–56] investigations. While we cite representative works, these references do not exhaust the extensive literature on the subject.

Thus, before the graphene era, an extensive body of research had firmly established trions as genuine Coulomb-

bound quasiparticles in quasi-two-dimensional systems, governed by universal few-body physics.

### III. FROM BULK AND QUANTUM-WELL SEMICONDUCTORS TO ATOMICALLY THIN MATERIALS

The historical development of trion physics in bulk and quantum-confined semiconductors laid the essential conceptual and methodological foundation for the modern resurgence of negatively and positively charged trions in atomically and molecularly thin materials. The discovery of graphene [57] and, subsequently, monolayer transition-metal dichalcogenides (TMDCs) [58] and Xenex, monolayers of group-IV elements such as Si, Ge, Sn revealed systems in which Coulomb interactions are dramatically enhanced due to extreme confinement, reduced dielectric screening, and tunable carrier densities. Xenex were first predicted theoretically [59, 60] and subsequently realized experimentally on substrates, beginning with silicene [61, 62] and followed by germanene [63] and stanene [64].

Despite graphene's central role in launching two-dimensional materials research, it does not support robust optical trions under typical conditions, owing to its gapless Dirac spectrum and strong dielectric screening. Although theoretical studies have predicted possible excitonic or trionic instabilities in graphene under extreme conditions—such as very strong magnetic fields, substrate-induced band gaps, or substantially reduced screening—these regimes are not representative of standard experimental settings. Consequently, graphene is best viewed as a bridge material: although it does not host robust trions itself, it motivated the exploration of gapped two-dimensional semiconductors, notably TMDCs and Xenex, where reduced screening and finite band gaps enable the stabilization and direct observation of both negatively and positively charged trions. In contrast to conventional quantum wells, these atomically thin materials exhibit trion binding energies reaching tens of meV, rendering trions stable even at room temperature. The dramatic resurgence of trion physics in TMDCs, Xenex, and other atomically thin monolayers after 2010 should therefore be understood not as a discovery *ex nihilo*, but as a natural continuation of more than five decades of theoretical and experimental research on Coulomb-bound few-body complexes in semiconductors.

### IV. CHARGED CARRIER INTERACTION IN 2D MONOLAYERS

Since the experimental discovery of highly conductive graphene monolayers in 2004 [57], the field of condensed matter physics has experienced explosive growth in theoretical and experimental research in the realm of 2D materials. The isolation of graphene from bulk crystals of graphite marked the identification of the first member of a family of 2D layered materials, which have grown rapidly over the past ten years and now includes insulators, semiconductors, semimetals, metals, and superconductors [65, 66]. 2D materials are commonly defined as crystalline materials consisting of a single layer of atoms. Most often, such materials are classified as either 2D allotropes of various elements or compounds consisting of two or more ionically/covalently bonded elements. These materials are crystalline solids with a high ratio between their lateral size and thickness [67]. In van der Waals layered materials, the atomic organization and bond strength in the 2D plane are typically much stronger than in the third dimension (out-of-plane), where they are bonded together by weak van der Waals interaction [66, 68]. Research on two-dimensional materials is primarily focused on graphene, transition-metal dichalcogenides, phosphorene, transition-metal trichalcogenides (TMTCs), and Xenex [69–73]. Among these, a particularly important and rapidly developing subclass is formed by buckled group-IV monolayers, collectively known as Xenex [74–76]. This family includes silicene [77], germanene [78], stanene [79], and borophene [80], which are distinguished by their tunable band gaps under externally applied electric fields and offer additional flexibility for electronic and optoelectronic applications.

The reduction of dimensionality has a profound and twofold effect on the interaction of charged particles in monolayer materials. First, if the electron–hole interaction is described by the Coulomb potential in a homogeneous dielectric environment and both charges are constrained to move in a plane, dimensional reduction affects the kinetic energy. In this case, the energy spectrum changes from the three-dimensional Rydberg series  $E_{3D} \sim 2\epsilon\hbar^2/n^2$  ( $n = 1, 2, \dots$ ) to the two-dimensional form  $E_{2D} \sim 2\epsilon\hbar^2/(n - 1/2)^2$ , resulting in a fourfold increase of the ground-state binding energy and reflecting the suppression of kinetic energy in two-dimensional excitons [81]. Secondly, more importantly, dimensional reduction also modifies the potential energy of the electron–hole interaction. While the interaction remains electromagnetic, dielectric screening in two dimensions differs fundamentally from the three-dimensional case. In a monolayer, polarization is confined to the plane, so that only the in-plane component of the induced electric field contributes to the interaction. As a result, the interaction remains a function of the in-plane separation  $r$  but acquires a functional form that differs substantially from the Coulomb potential. Figure 1 provides a schematic comparison between the electric field distribution of a dipole in a 3D bulk medium and the predominantly in-plane field lines characteristic of a dipole within a 2D monolayer.

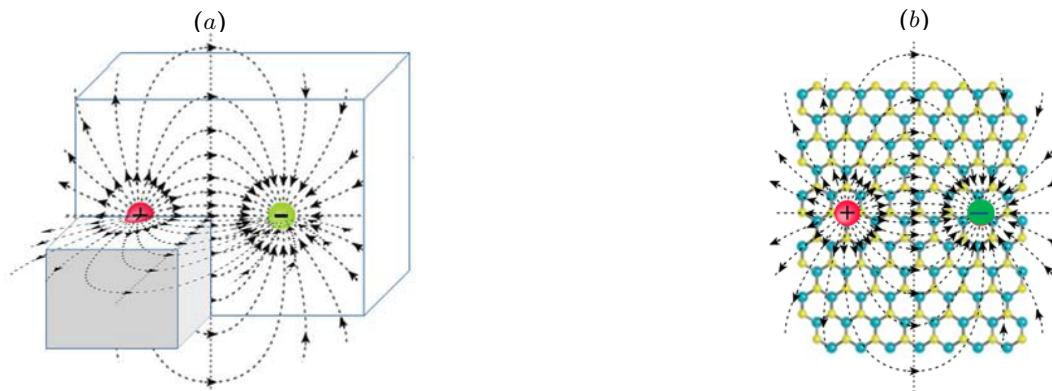


FIG. 1. Schematic representation of dipole electric fields in different dimensionalities. (a) The electric field of a dipole in a bulk 3D material. (b) Top-view schematic of a 2D monolayer, illustrating the in-plane electric field lines generated by an in-plane dipole. Fig. 1a adapted from [81].

The effective two-dimensional interaction between two point charges in a layered dielectric environment was derived by Rytova [82] and later by Keldysh [83]. A modern re-derivation and quantitative validation of the Rytova–Keldysh interaction, including its implications for excitonic states in atomically thin materials, was later provided within a rigorous dielectric screening framework [84]. This interaction, today known as the Rytova–Keldysh (RK) potential, is given by

$$V(r_{eh}) = -\frac{\pi k e^2}{(\varepsilon_1 + \varepsilon_2) \rho_0} \left[ H_0\left(\frac{r}{\rho_0}\right) - Y_0\left(\frac{r}{\rho_0}\right) \right]. \quad (1)$$

Here  $r$  is the in-plane electron–hole separation,  $k = 1/(4\pi\epsilon_0)$ ,  $H_0$  and  $Y_0$  are the Struve and Bessel functions of the second kind,  $\varepsilon_1$  and  $\varepsilon_2$  are the dielectric constants above and below the monolayer, and  $\rho_0 = 2\pi\zeta/[(\varepsilon_1 + \varepsilon_2)/2]$  is the screening length determined by the two-dimensional polarizability  $\zeta$ . The RK potential interpolates between a Coulomb tail  $V(r) \approx -ke^2/(\varepsilon r)$  for  $r \gg \rho_0$  and a logarithmic interaction  $V(r) \approx -\frac{ke^2}{\varepsilon\rho_0} \left[ \ln\left(\frac{r}{2\rho_0}\right) + \gamma \right]$  for  $r \ll \rho_0$ , where  $\gamma$  is the Euler constant. Thus, at short distances the  $1/r$  singularity is replaced by a much weaker logarithmic dependence.

Tuan et al. [85] critically examine the widely used Rytova–Keldysh potential for modeling Coulomb interactions in monolayer TMDCs. Although this potential has been extensively employed to describe excitons and trions in two-dimensional semiconductors, it does not consistently reproduce key experimental observations. Going beyond the conventional strictly 2D approximation, the authors [85] develop a microscopic description of the Coulomb interaction that explicitly incorporates the finite thickness and intrinsic three-atomic-sheet structure of TMDC monolayers, consisting of a metal layer sandwiched between two chalcogen layers. The derived effective potential accounts for the nonuniform dielectric environment, the out-of-plane spatial separation of charges, and the orbital character of the band-edge states. They demonstrate that the Coulomb interaction deviates from the simple logarithmic-to- $1/r$  crossover of the RK model, particularly at short distances relevant to excitons and trions. The refined screening modifies binding energies and fine-structure splittings, providing a physically transparent framework that bridges atomistic and effective-mass descriptions for more accurate modeling in realistic dielectric environments.

The Ref. [86] focused on experimental observations of dielectric-environment effects on the magnetic-field-induced brightening of neutral and charged dark excitons in monolayer WSe<sub>2</sub>, showing how encapsulation or substrate choice influences the optical visibility and activation of these spin-forbidden states. The authors demonstrated that incorporating realistic dielectric screening and finite-thickness effects is crucial for accurately modeling Coulomb interactions and excitonic complexes in monolayer semiconductors, thereby achieving improved quantitative agreement between theoretical predictions and experimental observations.

Taken together, the results of Refs. [85, 86] highlight the strong sensitivity of charge–charge interactions in two-dimensional materials to dielectric screening and confinement, thereby motivating the development of effective interaction potentials beyond the simple Coulomb form. In this context, modified Kratzer-type potentials, originally introduced in molecular physics by Kratzer [87], have been proposed as analytically tractable models for excitons in two-dimensional semiconductors [88]. In particular, this potential has been employed to model Rydberg excitons in dielectric environments, allowing the 2D Schrödinger equation to be solved exactly and yielding closed-form expressions for the eigenvalues and eigenfunctions [88–91]. Subsequent studies [90, 91] demonstrated that the modified Kratzer potential admits exact solutions in two dimensions and can be systematically applied to excitonic systems in

layered semiconductors.

The modified Kratzer potential takes the form [88]

$$V(r) = -\frac{1}{4\pi\epsilon_0} \frac{e^2}{\tilde{\rho}_0} \left( \frac{r_0}{r} - g^2 \frac{r_0^2}{r^2} \right), \quad (2)$$

where  $\epsilon_0$  is the vacuum permittivity,  $\tilde{\rho}_0 = r_0\epsilon$  is the effective screening length, and  $\epsilon$  is the dielectric constant of the surrounding medium. This potential interpolates between different interaction regimes: for  $r_0 = 1$  and  $g = 0$  it reduces to the Coulomb potential, while  $g^2 = 1/2$  reproduces the original Kratzer potential [87].

The analytical solvability of the Kratzer-type potential (2) makes it a powerful tool for modeling electron–hole, electron–electron, and hole–hole interactions in low-dimensional systems, in particular, to study  $X^-$  and  $X^+$  trions. A series of recent works has applied this approach to excitons and related bound states in two-dimensional semiconductors, including TMDC monolayers, demonstrating that it captures essential features of exciton binding and dielectric screening while permitting exact or nearly exact solutions of the Schrödinger equation [89, 91]. Moreover, the modified Kratzer model has been used as a basis for analytical estimates of exciton and trion binding energies and for describing long-range interaction effects in layered materials, providing a useful complement to more microscopic approaches [88, 90, 91].

## V. EXPERIMENTAL OBSERVATION OF TRIONS IN 2D MONOLAYERS

### A. Trions in TMDC

The experimental investigation of trions in TMDC monolayers began shortly after the discovery of strongly bound excitons in these atomically thin semiconductors. The first unambiguous experimental measurements of trion binding energies were reported in 2013 using low-temperature optical spectroscopy [92, 93]. In these early studies, photoluminescence (PL) spectra of the monolayer MoS<sub>2</sub> and MoSe<sub>2</sub> revealed an additional emission peak at energies below the exciton resonance. This feature was identified as a charged exciton, formed by binding an exciton with an extra electron or hole.

The trion binding energy is experimentally extracted from the energy splitting between the neutral exciton and trion peaks,  $E_b = E(X^0) - E(X^\pm)$ . For monolayer MoS<sub>2</sub>, the first measurements yielded  $E_b \simeq 18\text{--}20$  meV [92], already an order of magnitude larger than typical trion binding energies in conventional semiconductor quantum wells. This immediately highlighted the crucial role of reduced dimensionality and weak dielectric screening in enhancing Coulomb interactions in 2D materials.

**Experimental methods.** The dominant experimental techniques used to probe trions in TMDC monolayers are optical in nature. Low-temperature PL spectroscopy remains the most widely employed method, owing to its sensitivity and relative simplicity. Complementary information is obtained from reflectance contrast and absorption spectroscopy, which directly probe excitonic resonances [94, 95]. In many experiments, electrostatic gating in field-effect transistor geometries is used to tune the carrier density and control the charge state of the excitonic complexes [93, 96]. This approach allows the selective formation of negative trions,  $X^-$ , in electron-doped regimes and positive trions,  $X^+$ , in hole-doped regimes, providing clear experimental confirmation of both species.

**Identification of  $X^-$  and  $X^+$  trions.** Gate-dependent PL measurements established that the trion peak evolves systematically with doping polarity. In monolayer MoSe<sub>2</sub> and WSe<sub>2</sub>, both  $X^-$  and  $X^+$  trions were observed, with binding energies typically in the range of 25–40 meV [93, 96]. In many cases, the binding energies of positive and negative trions are comparable, although small asymmetries are sometimes resolved and attributed to differences in effective masses and band structure. When charge discrimination is not experimentally possible, the reported binding energy corresponds to the charged exciton peak without explicit identification of its sign.

**Material dependence.** Systematic experimental studies revealed clear trends across the TMDC family. Mo-based monolayers such as MoS<sub>2</sub> and MoSe<sub>2</sub> typically exhibit trion binding energies in the range  $\sim 18\text{--}30$  meV [92, 93]. W-based materials, including WS<sub>2</sub> and WSe<sub>2</sub>, generally show larger values, often extending up to  $\sim 40$  meV [94, 96, 97]. This enhancement is commonly attributed to stronger spin–orbit coupling and heavier carrier effective masses. In contrast, monolayer MoTe<sub>2</sub> exhibits somewhat smaller trion binding energies, typically  $\sim 14\text{--}27$  meV, reflecting increased dielectric screening and a reduced band gap [98, 99].

**Role of dielectric environment and disorder.** A key experimental finding is the strong sensitivity of trion binding energies to the surrounding dielectric environment. Comparisons between monolayers on SiO<sub>2</sub>, encapsulated in hBN, or suspended demonstrate that increased screening reduces the measured binding energy, while encapsulation narrows spectral linewidths and improves sample quality [86, 95]. As a result, experimentally reported trion binding energies often span a range rather than a single universal value for a given material.

**Temperature and carrier-density effects.** Trion resonances are robust at low temperatures and, in some materials, persist up to room temperature, albeit with significant broadening [92, 100]. The first clear experimental observation of tightly bound trions in monolayer MoS<sub>2</sub> by Mak *et al.* [92] demonstrated that the trion binding energy remains sufficiently large to survive thermal fluctuations at 300 K. Subsequent temperature-dependent photoluminescence studies have shown that while exciton and trion resonance energies redshift with increasing temperature due to electron–phonon interactions, the exciton–trion energy separation exhibits weak or moderate temperature dependence depending on the material system [93, 101, 102]. Increasing carrier density leads to enhanced screening and a gradual reduction of the exciton–trion energy splitting [92, 103]. At sufficiently high doping levels, the optical response crosses over to an exciton–polaron regime, reflecting the many-body nature of the electron–exciton interaction [104].

**Experimental significance.** The experimental discovery and systematic characterization of trions in TMDC monolayers established these materials as a unique platform for studying few-body and many-body Coulomb-correlated states in two dimensions. The unusually large trion binding energies, combined with tunability via gating, substrate engineering, and temperature, have made trions a central element of the optical response of TMDCs and a benchmark for theoretical three-body and polaronic descriptions of excitonic complexes in reduced dimensionality.

Different experimental groups [86, 92–94, 105–125] observed and reported the signature of a trion in TMDCs formed from a hole in the first valence band and electrons originating predominantly from downwards curved conduction bands of the  $K$  and/or  $K'$  valleys. The reported trion binding energies depend on dielectric screening (substrate versus hBN encapsulation), carrier density, and temperature.

We summarize experimentally measured trion binding energies in TMDCs, as extracted from different experimental methods of measurement (photoluminescence, reflectance contrast, and gate-dependent optical spectroscopy). Table I summarizes representative experimental trion binding energies reported for monolayer semiconducting group-VI TMDCs. Nevertheless, experimental values for monolayer TMDCs consistently fall in the range  $E_b \sim 20$ –40 meV, as shown in Fig. 2, reflecting enhanced Coulomb interactions in 2D systems.

## B. Trions in anisotropic monolayers

Trions in phosphorene (monolayer of black phosphorus) have been investigated both experimentally and theoretically, revealing a rich and anisotropic few-body physics distinct from that of isotropic two-dimensional semiconductors. Experimental studies have reported clear signatures of negatively charged trions through photoluminescence spectroscopy in monolayer and few-layer phosphorene, demonstrating optical tunability via photoexcitation and gating [126]. Subsequent experiments revealed extraordinarily large trion binding energies in few-layer phosphorene,

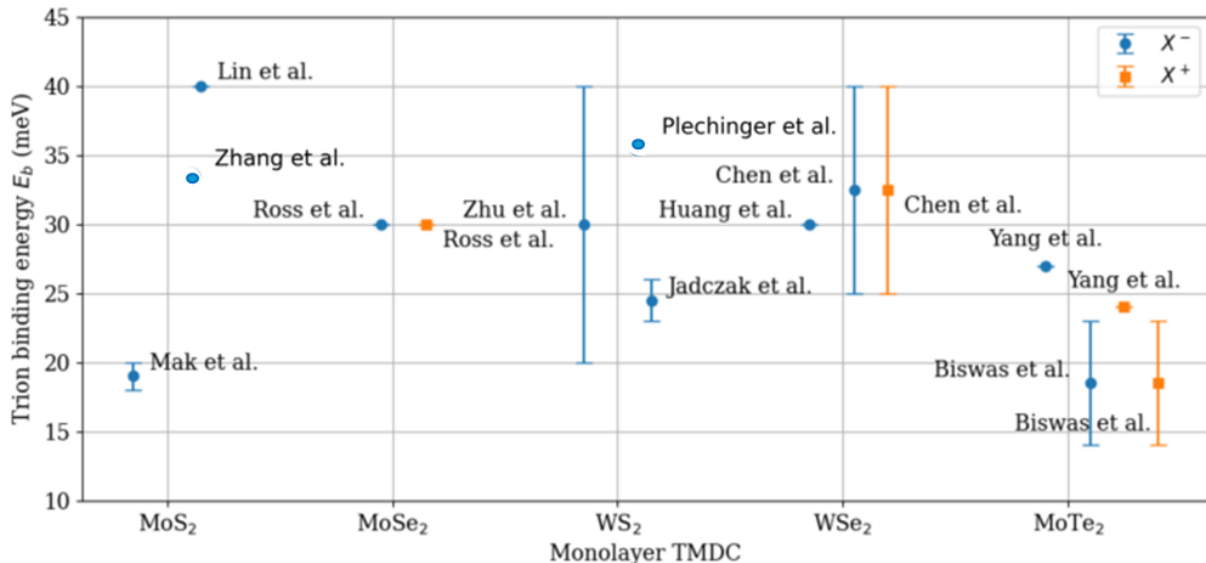


FIG. 2. Typical experimentally measured trion binding energies  $E_b$  in monolayer TMDCs from low-temperature optical spectroscopy. Points indicate representative mean values; error bars show reported experimental ranges, reflecting variations in dielectric environment, substrate, and carrier density. Experimental trion binding energies in monolayer TMDCs are taken from Refs. [92–99, 105–107].

TABLE I. Experimentally measured trion binding energies  $E_b$  in monolayer TMDCs. Binding energies are typically extracted from the energy separation between the neutral exciton ( $X^0$ ) and charged trion ( $X^\pm$ ) peaks in optical spectra.

Material	Trion type	$E_b$ (meV)	Experimental reference
MoS <sub>2</sub>	$X^-$	18–20	Mak <i>et al.</i> [92]
MoS <sub>2</sub>	$X^-$	~40	Lin <i>et al.</i> [105]
MoSe <sub>2</sub>	$X^-$	~30	Ross <i>et al.</i> [93]
MoSe <sub>2</sub>	$X^+$	~30	Ross <i>et al.</i> [93] <sup>a</sup>
WS <sub>2</sub>	$X^-$	20–40	Zhu <i>et al.</i> [94]
WS <sub>2</sub>	$X^-$	23–26	Jadczak <i>et al.</i> [95]
WSe <sub>2</sub>	$X^-$	~30	Huang <i>et al.</i> [97]
WSe <sub>2</sub>	$X^+$	25–40	Chen <i>et al.</i> [96]
WSe <sub>2</sub>	$X^-$	25–40	Chen <i>et al.</i> [96]
MoTe <sub>2</sub>	$X^+$	~24	Yang <i>et al.</i> [98]
MoTe <sub>2</sub>	$X^-$	~27	Yang <i>et al.</i> [98]
MoTe <sub>2</sub>	$X^+$	14–23	Biswas <i>et al.</i> [99] <sup>a</sup>
MoTe <sub>2</sub>	$X^-$	14–23	Biswas <i>et al.</i> [99] <sup>a</sup>

<sup>a</sup> In these experiments,  $X^+$  and  $X^-$  trions are not spectrally resolved with sufficient accuracy.

attributed to its quasi-one-dimensional electronic structure and reduced dielectric screening [127, 128]. More recently, electrically controlled excitonic complexes, including trions, were observed in high-quality bilayer phosphorene devices, confirming the stability of charged excitons in gated and encapsulated samples [129].

Due to reduced dimensionality, weak dielectric screening, and strong in-plane anisotropy, excitons and trions in monolayer phosphorene exhibit pronounced quasi-one-dimensional (quasi-1D) behavior. As a result, their binding energies are substantially larger than those observed in quasi-two-dimensional quantum wells and in more isotropic 2D materials such as TMDCs. An exceptionally large trion binding energy of approximately 100 meV was first reported in monolayer phosphorene [128], which is about two to five times larger than typical values in tungsten- or molybdenum-based TMDC monolayers. Even higher trion binding energies have been observed in few-layer phosphorene: experiments on three-layer phosphorene deposited on a SiO<sub>2</sub>/Si substrate revealed ultrahigh binding energies of up to 162 meV, attributed to the formation of quasi-1D trions in the intrinsically anisotropic 2D phosphorene lattice [127].

Recent experimental studies have substantially refined the understanding of trion binding energies in phosphorene, revealing both large absolute values and a pronounced sensitivity to dimensionality and environment. Early photoluminescence measurements reported trion binding energies of approximately 100 meV [128] in monolayer phosphorene on SiO<sub>2</sub>/Si substrates [126], while few-layer systems, such as three-layer phosphorene, exhibit even larger quasi-1D trion binding energies in the range of 160–180 meV [127]. More recent experiments have provided further insight: Molas *et al.* [130] observed trion binding energies near 120 meV in monolayer phosphorene (the extracted binding energy of the trion in triple layer black phosphorus is on the order of 160 meV, which is a larger value compared to the case of the monolayer (100–120 meV) reported in Refs. [126, 131]) using photoluminescence spectroscopy, whereas Yoon *et al.* [129] identified an additional trion resonance approximately 30 meV below the neutral exciton under electrostatic gating. Complementary theoretical analyses and refined experimental interpretations suggest that, when referenced appropriately to specific excitonic states, the effective trion binding energy under certain conditions may be closer to 70 meV, underscoring the strong dependence of trion binding energies on dielectric screening, layer thickness, and charge density [132]. Calculations [133] indicate that, when substrate-induced screening is fully accounted for, the effective trion binding energy in certain few-layer configurations is reduced to approximately 70 meV, offering a more physically consistent description of the observed variability.

Related to the experimental search for trions in other anisotropic monolayers, transition-metal trichalcogenides (TMTCs, MX<sub>3</sub>) have emerged over the past decade as an important class of low-dimensional materials. Among recently developed two-dimensional systems, only a limited number exhibit strong in-plane structural anisotropy, notably TMTCs such as TiS<sub>3</sub>, TiSe<sub>3</sub>, ZrS<sub>3</sub>, and ZrSe<sub>3</sub>. While TiS<sub>3</sub> is a direct-gap semiconductor in the monolayer limit, TiSe<sub>3</sub>, ZrS<sub>3</sub>, and ZrSe<sub>3</sub> are predicted to remain indirect-gap materials [134, 135]. The crystal structures and characteristic mechanical, electronic, optical, magnetic, and charge-density-wave transport properties of TMTCs have been comprehensively reviewed elsewhere [136, 137]. Experimentally, optical studies of TMTCs have revealed pronounced excitonic effects and strong photoluminescence anisotropy, including polarization-resolved photoluminescence in ZrS<sub>3</sub> and visible emission from HfS<sub>3</sub> nanoribbons, while excitonic contributions have been invoked to explain large birefringence and linear dichroism in TiS<sub>3</sub> and related compounds [138]. However, in contrast to the well-established gate-tunable trion spectroscopy in transition-metal dichalcogenide monolayers, unambiguous experimental identifica-

tion of trions in monolayer TMTCs—via controlled charge doping and clearly resolved exciton–trion splitting—remains scarce.

At present, evidence for trion states in TMTCs is primarily supported by theoretical studies, including explicit calculations of excitons and trions in monolayer  $\text{TiS}_3$  [139], which suggest that these complexes should be stable. Consequently, targeted gate-dependent optical experiments in high-quality, encapsulated TMTC devices represent a critical open direction for the field and would provide the necessary evidence to confirm the predicted few-body physics in these anisotropic systems.

### C. Trions in Xenex

Trions are well established experimentally in direct-gap 2D semiconductors such as TMDC monolayers, where they are typically identified through gate-controlled carrier doping and a clearly resolved exciton–trion splitting in photoluminescence and/or reflectance spectra. In contrast, for Xenex—buckled group-IV monolayers such as silicene, germanene, and stanene—unambiguous experimental observation of trions remains limited. A key practical limitation is that these materials are commonly realized epitaxially on metallic templates, where strong hybridization and screening can substantially modify (or suppress) intrinsic optical responses and hinder clean charge-tunable exciton spectroscopy [140–142]. As a result, trions in Xenex have been investigated predominantly at the theoretical level, including predictions of electrically tunable trion binding energies and related many-body effects in silicene, germanene, and stanene under perpendicular electric fields [143, 144]. While functionalized Xenex (e.g., germanane and related derivatives) exhibit measurable photoluminescence and excitonic photophysics, systematic gate-dependent studies establishing charged-exciton resonances in the same definitive manner as TMDCs are still largely missing [145, 146]. These considerations indicate that high-quality, encapsulated, charge-tunable Xene devices on insulating substrates would be essential for a definitive experimental trion spectroscopy in this material family.

Theoretical studies of excitons and magnetoexcitons have demonstrated that the binding energies and optical properties of both direct and indirect excitonic states can be strongly tuned by external electric and magnetic fields [147, 148]. These works showed that the interplay between field-induced band-structure modifications and the RK interaction leads to significant control of excitonic spectra, including Rydberg states and diamagnetic coefficients, suggesting potential applications in electrically and magnetically tunable optoelectronic devices. Similar approaches can be extended to the study of trions in Xenex.

## VI. THEORETICAL APPROACHES AND FORMALISM

This section summarizes the general low-energy formalism used to describe Mott–Wannier trions in two-dimensional materials within the framework of the non-relativistic approach. We introduce the effective three-body Hamiltonian, employ mass-scaled Jacobi coordinates to separate the center-of-mass (*c.m.*) motion, and derive the Schrödinger equation governing the relative motion of the three charged particles. Throughout this work, Mott–Wannier trions in a two-dimensional semiconductor are modeled within the isotropic effective-mass approximation. The electrostatic interactions between electrons and holes are assumed to be isotropically screened by the static dielectric permittivity of the crystal. A trion is treated as a three-particle bound state: a negatively charged trion,  $X^-$ , consists of two electrons and one hole, whereas a positively charged trion,  $X^+$ , consists of two holes and one electron. Within this framework, the non-relativistic Mott–Wannier trion Hamiltonian in a 2D plane is given by

$$H = - \sum_{i=1}^3 \frac{\hbar^2}{2m_i} \nabla_i^2 + \sum_{i<j}^3 V_{ij}(|\mathbf{r}_i - \mathbf{r}_j|), \quad (3)$$

where  $m_i$  and  $\mathbf{r}_i$  denote the effective mass and the in-plane position vector of the  $i$ th particle, respectively. Electrons and holes are treated within the band effective-mass approximation. The interaction potential  $V_{ij}$  describes the screened Coulomb interaction between charged carriers in a 2D material. Depending on the level of approximation, it can be modeled by the Rytova–Keldysh (1), modified Kratzer-type (2) potentials, or other effective screened interaction forms such as those introduced in Ref. [85]. Since the Hamiltonian (3) is invariant under two-dimensional rotations, the total orbital angular momentum  $J$  is conserved and therefore a good quantum number.

The corresponding Schrödinger equation for the three-particle system reads

$$\left[ - \sum_{i=1}^3 \frac{\hbar^2}{2m_i} \nabla_i^2 + \sum_{i<j}^3 V_{ij}(|\mathbf{r}_i - \mathbf{r}_j|) \right] \Psi(\mathbf{r}_1, \mathbf{r}_2, \mathbf{r}_3) = \mathcal{E} \Psi(\mathbf{r}_1, \mathbf{r}_2, \mathbf{r}_3). \quad (4)$$

In crystalline solids, the effective mass of charge carriers is determined by the local curvature of the electronic band dispersion evaluated at a band extremum (valley),  $(m_\alpha^*)^{-1} = \frac{1}{\hbar^2} \frac{\partial^2 E(\mathbf{k})}{\partial k_\alpha^2} \Big|_{\mathbf{k}=\mathbf{k}_0}$  [149, 150], where  $\mathbf{k}_0$  denotes the position of the valley in the Brillouin zone and  $\alpha$  labels the Cartesian components. Consequently, when different valleys correspond to inequivalent points in the Brillouin zone, their band curvatures—and therefore the corresponding effective masses—can differ. In two-dimensional materials, this leads to a valley dependence of the electron and hole effective masses that are both material- and band-specific.

In monolayer TMDCs, the K and K' valleys are related by time-reversal symmetry and thus possess identical effective masses for electrons and holes [69, 151, 152]. By contrast, other valleys, such as the Q valleys in the conduction band or the  $\Gamma$  point in the valence band, are inequivalent and often characterized by distinct and anisotropic effective masses, which can become relevant at elevated carrier densities, under applied strain, or in multilayer structures [69].

The valley dependence of effective masses has important consequences for the fine structure of trions in two-dimensional materials. For intravalley trions formed from carriers near the K and K' valleys, the equality of effective masses ensures valley-degenerate binding energies in the absence of external fields. However, for intervalley trions or trions involving carriers from inequivalent valleys (e.g., K–Q or  $\Gamma$ –K configurations), differences in effective masses modify the reduced masses entering the three-body Hamiltonian (3). This leads to distinct trion binding energies, altered level ordering, and valley-dependent exchange splittings [153–155]. Such effects contribute to the experimentally observed richness of trion spectra and their sensitivity to doping, strain, and dielectric environment.

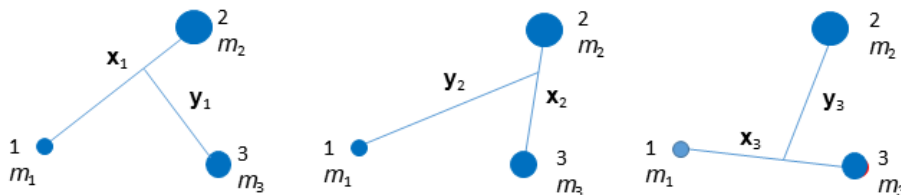


FIG. 3. Schematic illustration of the mass-scaled Jacobi coordinates set for three nonidentical particles forming a trion.

Therefore, in general, the particle masses  $m_i$  appearing in Eqs. (3) and (4) are not identical, reflecting the possible differences between electron and hole effective masses and, in some cases, their valley or band dependence. As a consequence, an explicit separation of the *c.m.* motion from the internal dynamics of the three-body system is required. To this end, we introduce mass-scaled Jacobi coordinates shown in Fig. 3. For a given partition  $i$  ( $i \neq j \neq k = 1, 2, 3$ ), these coordinates are defined as

$$\begin{aligned} \mathbf{x}_i &= \sqrt{\frac{m_j m_k}{(m_j + m_k)\mu}} (\mathbf{r}_j - \mathbf{r}_k), \\ \mathbf{y}_i &= \sqrt{\frac{m_i(m_j + m_k)}{(m_1 + m_2 + m_3)\mu}} \left( \mathbf{r}_i - \frac{m_j \mathbf{r}_j + m_k \mathbf{r}_k}{m_j + m_k} \right), \\ \mathbf{R} &= \frac{m_1 \mathbf{r}_1 + m_2 \mathbf{r}_2 + m_3 \mathbf{r}_3}{M}, \quad M = m_1 + m_2 + m_3, \end{aligned} \quad (5)$$

where  $\mathbf{R}$  is the *c.m.* coordinate and

$$\mu = \sqrt{\frac{m_1 m_2 m_3}{m_1 + m_2 + m_3}} \quad (6)$$

is the three-particle effective mass.

After the transformation to Jacobi coordinates, the *c.m.* motion separates, and the Schrödinger equation for the relative motion of the three-body system becomes

$$\left[ -\frac{\hbar^2}{2\mu} (\nabla_{\mathbf{x}_i}^2 + \nabla_{\mathbf{y}_i}^2) + \sum_{i < j}^3 V_{ij} - \mathcal{E} \right] \Psi(\mathbf{x}_i, \mathbf{y}_i) = 0. \quad (7)$$

Equation (7) governs the internal dynamics of two-dimensional trions and forms the starting point for further analysis, including solutions based on a variety of few-body approaches discussed in the following subsections.

## A. Deterministic Few-Body Methods

Below, we consider the variational method, stochastic variational method, exact (direct) diagonalization, and Gaussian expansion method. The common foundation of these approaches is the variational principle, which guarantees that any properly normalized trial wave function yields an upper bound to the exact ground-state energy. By refining the functional form of the wave function or enlarging the basis set, these deterministic approaches systematically converge toward the exact solution within the effective-mass approximation. In two-dimensional materials, where the Rytova–Keldysh potential introduces nontrivial screening effects and strong carrier correlations, deterministic frameworks are essential for achieving high numerical precision. In these methods, the Schrödinger equation is solved by expanding the wave function in a suitable basis and determining the eigenvalues through variational optimization or matrix diagonalization. In the following subsections, we review four deterministic approaches applied to trions in 2D materials: the variational method, the stochastic variational method with explicitly correlated Gaussians, exact diagonalization, and the Gaussian expansion method.

### 1. Variational method

The variational method (VM) is a powerful and systematically improvable approach for obtaining accurate approximations to bound-state solutions of few-body quantum systems. Its foundation lies in the Rayleigh–Ritz principle, according to which the expectation value of the Hamiltonian operator,

$$\mathcal{E}[\Psi] = \frac{\langle \Psi | \hat{H} | \Psi \rangle}{\langle \Psi | \Psi \rangle}, \quad (8)$$

provides an upper bound to the exact ground-state energy for any normalized trial wave function  $\Psi$  that satisfies the required symmetry and boundary conditions.

In the framework of VM the trial wave function is constructed as a linear superposition of basis states,

$$\Psi = \sum_{i=1}^N c_i \Phi_i, \quad (9)$$

where  $\{\Phi_i\}$  denotes a chosen set of basis functions and  $\{c_i\}$  are variational coefficients to be determined. Substituting this expansion into the functional  $E[\Psi]$  and minimizing with respect to the coefficients  $c_i$  leads to a generalized eigenvalue problem,

$$\sum_{j=1}^N (H_{ij} - \mathcal{E} S_{ij}) c_j = 0, \quad (10)$$

where

$$H_{ij} = \langle \Phi_i | \hat{H} | \Phi_j \rangle, \quad S_{ij} = \langle \Phi_i | \Phi_j \rangle \quad (11)$$

are the Hamiltonian and overlap matrices, respectively.

The accuracy of the variational solution depends on the completeness and flexibility of the chosen basis. Increasing the basis size  $N$  or introducing additional nonlinear variational parameters systematically improves the approximation and ensures convergence of the energy from above toward the exact value. In practice, convergence is monitored by examining the stability of the eigenvalues with respect to variations of the basis parameters and by verifying the saturation of relevant observables.

In addition to providing reliable ground-state energies, the variational framework allows for the computation of structural properties such as root-mean-square radii, correlation functions, and probability densities, which can be evaluated directly using the optimized wave function. The method is particularly well suited for few-body systems, where high numerical precision can be achieved with a relatively moderate basis size or trial wave functions.

The seminal 2013 paper by Berkelbach, Hybertsen, and Reichman [156] provided the first comprehensive variational calculations for trions in TMDC monolayers using the Rytova–Keldysh potential. In Ref. [157], high-precision variational calculations of trions in TMDCs were performed using trial wave functions constructed from two-dimensional Slater-type orbitals in the form introduced in Ref. [158]. The variational trion wave function was expressed as a linear combination of products of Slater-type orbitals. The authors in Ref. [159] also provided a comprehensive review of theoretical studies on the structure and binding energies of localized excitons and trions in nanosystems within the variational framework (see also references therein).

## 2. Stochastic Variational Method

The stochastic variational method (SVM) provides high-precision solutions of few-body quantum systems by expanding the many-body wave function in a flexible basis of explicitly correlated Gaussians (ECGs) [160]. The method has been extensively validated for atomic, molecular, nuclear, and excitonic few-particle systems and is particularly well suited for treating both ground and excited states of excitons, trions, and biexcitons in reduced dimensions.

Within the effective-mass approximation, for trions consisting of three particles confined to a 2D plane described by the nonrelativistic Hamiltonian (3), the variational wave function is expanded in a basis of ECGs [161],

$$\Psi = \sum_{k=1}^K c_k \mathcal{A} \left\{ \chi_{\text{spin}}^S \left[ \prod_{i=1}^3 \xi_{m_i}(\mathbf{r}_i) \exp \left( -\frac{1}{2} \sum_{i,j=1}^3 A_{ij} \mathbf{r}_i \cdot \mathbf{r}_j \right) \right] \right\}, \quad (12)$$

with the angular prefactor

$$\xi_m(\mathbf{r}) = (x + iy)^m, \quad (13)$$

where  $\mathcal{A}$  is the antisymmetrization operator acting on identical fermions,  $\chi_{\text{spin}}^S$  is spin function coupling the electrons' and holes' spins to total spin  $S$ , and the set of nonlinear parameters  $\{A_{ij}\}$  defines the Gaussian widths and correlations. The nonlinear variational parameters are optimized using the stochastic variational method [160, 161]. The total angular momentum in two dimensions is  $\mathcal{L} = \sum_{i=1}^3 l_i$  with projection  $\mathfrak{M} = \mathbf{m}_1 + \mathbf{m}_2 + \mathbf{m}_3$ , the integers  $\mathbf{m}_i$  determine the angular momentum projection. The spatial wave function in Eq. (12) is coupled with the spin function  $\chi_{SM}^S$  to form the complete trial wave function.

The ECG basis efficiently captures both strong short-range correlations and extended spatial structures, making it well suited for weakly bound and excited excitonic complexes. The nonlinear parameters are optimized stochastically by retaining only basis functions that lower the total energy, allowing the basis to adapt to the dominant correlations while maintaining numerical stability. ECGs are widely used in nuclear and atomic physics, and quantum chemistry [160] due to: i. the analytical availability of matrix elements; ii. high variational flexibility; iii. straightforward treatment of permutation symmetry; iv. simple coordinate transformations.

Material-dependent parameters, such as effective masses and screening lengths, are taken from *ab initio*-based parameterizations known to reproduce exciton binding energies in good agreement with Bethe–Salpeter calculations. For simplicity, and in accordance with experimental observations, calculations are often performed assuming equal electron masses in  $X^-$  and hole masses in  $X^+$ , which ensures charge-conjugation symmetry between positive and negative trions without affecting the qualitative behavior of the binding energies. The calculated exciton binding energies are found to be in good agreement with experimental values, typically on the order of several hundred millielectronvolts in monolayer transition metal dichalcogenides. Trions [162, 163] and biexciton [164] binding energies are also well reproduced within this framework, demonstrating the reliability of the effective-mass model combined with the SVM for three-body excitonic complexes.

## 3. Exact Diagonalization Method

The exact diagonalization (ED) method, also referred to as direct diagonalization, provides a nonperturbative approach to few-body excitonic complexes by representing the Hamiltonian in a finite basis and solving the resulting matrix eigenvalue problem numerically. In the context of trions in 2D semiconductors, the method is typically implemented within the effective-mass approximation, employing screened Coulomb interactions modeled via the Rytova–Keldysh potential to account for non-local screening effects.

To make the problem tractable, after separating the *c.m.* motion, the relative three-body wave function  $\Psi(\mathbf{x}, \mathbf{y})$ , in Jacobi coordinates, is expanded in a finite basis set of dimension  $N_b$ :

$$\Psi(\mathbf{x}, \mathbf{y}) = \sum_{n=1}^{N_b} c_n \Phi_n(\mathbf{x}, \mathbf{y}). \quad (14)$$

Typical choices for the basis functions  $\{\Phi_n\}$  include 2D harmonic-oscillator states, plane waves, or specialized Gaussian-type orbitals. The Hamiltonian matrix elements,  $H_{mn} = \langle \Phi_m | \hat{H} | \Phi_n \rangle$ , are computed explicitly, leading to a finite-dimensional eigenvalue problem:

$$\mathbf{H}\mathbf{c} = \mathcal{E}\mathbf{c}. \quad (15)$$

Diagonalization of the matrix eigenvalue problem (15) yields the discrete energy spectrum, providing direct access to both ground and excited states, as well as the corresponding wave functions. The method is numerically exact within the chosen finite basis. However, exact diagonalization (ED) suffers from the “curse of dimensionality,” since the basis size required for convergence grows rapidly—typically exponentially—with the number of particles  $N$ , which typically limiting the method to  $N \leq 4$ .

If the system possesses rotational symmetry, as is commonly the case for the ground state of a trion, the total angular momentum can be separated. In this situation, the wave function may be decomposed into angular and radial parts, and the basis expansion is performed over the radial component only. The resulting basis functions then depend solely on the magnitudes of the Jacobi coordinates and the relative angle between them.

The ED approach has been applied to exciton–electron systems in configuration space [165] and to the study of trions in TMDC using a momentum-space formulation [166]. Notably, ED provides a vital deterministic benchmark for Monte Carlo approaches such as diffusion Monte Carlo and path-integral Monte Carlo.

#### 4. Gaussian Expansion Method

Over the past two decades, the Gaussian expansion method (GEM), which is based on a systematic expansion of the wave function in Gaussian basis functions, has been widely and successfully applied to few-body systems in nuclear physics for the precise description of three- and four-particle systems; see, for example, Refs. [167–172]. The GEM is a deterministic variational technique for solving few-body Schrödinger equations in configuration space. Most recently GEM was applied to investigate the properties of trions in TMDCs monolayers [173]. After separating the *c.m.* motion, the trion wave function is written in Jacobi coordinates and expanded over a finite set of Gaussian basis states, often organized into *rearrangement channels* (different Jacobi partitions) to efficiently capture alternative correlation topologies (e.g., an exciton plus a spectator carrier). In a compact form, the variational ansatz for a state with total orbital angular momentum  $J$  can be written as [173]

$$\Psi^J(\mathbf{x}, \mathbf{y}) = \sum_i \sum_{\alpha_i} A_{\alpha_i}^i \Phi_{\alpha_i}^i(\mathbf{x}_i, \mathbf{y}_i), \quad (16)$$

where  $(\mathbf{x}_i, \mathbf{y}_i)$  are the Jacobi coordinates in partition  $i$ ,  $\alpha_c$  labels the quantum numbers and nonlinear width parameters of the Gaussian basis, and  $A_{\alpha_i}^i$  are linear expansion coefficients [173].

In each channel, the basis functions are constructed from Gaussian radial factors (with widths chosen in a geometric progression to cover both short- and long-range length scales) multiplied by angular functions that carry the total angular momentum  $J$ . Substituting Eq. (16) into the Schrödinger equation and applying the Rayleigh–Ritz variational principle leads to a generalized secular equation for eigenvalue problem with Hamiltonian in Jacobi coordinates from Eq. (7) and corresponding overlap matrices.

Diagonalization of secular equation yields the discrete spectrum and wave functions. Because GEM is variational, the computed energies are upper bounds to the exact eigenvalues within the assumed Hamiltonian, and convergence is systematically improved by enlarging the basis and/or the set of channels.

Although both GEM and the SVM employ Gaussian basis functions, their philosophies differ fundamentally. In GEM, the nonlinear Gaussian width parameters are fixed in advance using a deterministic geometric progression, and convergence is achieved by increasing the basis size across multiple rearrangement channels. In contrast, SVM uses explicitly correlated Gaussians whose nonlinear parameters are optimized stochastically through iterative energy minimization. This adaptive optimization allows SVM to capture interparticle correlations more efficiently with fewer basis functions, often achieving benchmark-level precision. GEM, however, is computationally simpler and fully deterministic, whereas SVM requires nonlinear optimization but provides greater flexibility in describing correlated few-body dynamics.

In the framework of deterministic approaches, the trion binding energy is extracted by comparing the trion ground-state energy to that of the isolated exciton:

$$\mathcal{E}_b(X^\pm) = \mathcal{E}(X) - \mathcal{E}(X^\pm), \quad (17)$$

where  $\mathcal{E}(X)$  and  $\mathcal{E}(X^\pm)$  are obtained independently using the same basis framework with the exciton and trion Hamiltonians, respectively, to ensure consistent error cancellation. These methods serve as the primary validation for diffusion Monte Carlo and path-integral Monte Carlo results, particularly in the few-body limit where basis convergence is attainable.

To conclude, deterministic approaches—most notably the SVM, GEM, and ED, provide high-precision benchmarks for few-body excitonic complexes. By representing the Hamiltonian in a basis set and solving the resulting equations, these methods bypass the statistical noise inherent in Monte Carlo techniques.

## B. Quantum Monte Carlo methods

Quantum Monte Carlo (QMC) [174, 175] is an umbrella term for stochastic numerical methods used to solve quantum many-body problems by Monte Carlo sampling. It includes several approaches that differ in formulation and target observables. Diffusion Quantum Monte Carlo (DMC) [175, 176] is a zero-temperature QMC method that projects out the exact ground state by evolving a trial wave function in imaginary time. For fermionic systems, it relies on the fixed-node approximation to mitigate the fermion sign problem by imposing nodal constraints, as the problem remains fundamentally unsolved and has been shown to be computationally NP-hard [177] for general fermionic systems.

In contrast, path-integral Monte Carlo (PIMC) [178–180] is a finite-temperature QMC method based on the imaginary-time path-integral representation of the density matrix, which samples thermal ensembles without an explicit trial wave function and provides direct access to thermodynamic quantities. While DMC is most effective for zero-temperature fermionic systems, PIMC naturally includes thermal effects but becomes severely limited by the fermion sign problem at low temperatures.

### 1. Diffusion Monte Carlo for 2D trions

Diffusion Quantum Monte Carlo is a stochastic projector method designed to extract the ground-state properties of many-body systems. The method is based on the observation that the Schrödinger equation in imaginary time,  $\tau = it$ , takes the form of a generalized diffusion equation. For a system described by the Hamiltonian (3), the evolution of a trial wave function  $\Psi_T$  is given by:

$$-\frac{\partial \Psi(\mathbf{R}, \tau)}{\partial \tau} = (\hat{H} - \mathcal{E}_T) \Psi(\mathbf{R}, \tau), \quad (18)$$

where  $\mathbf{R} = (\mathbf{r}_1, \mathbf{r}_2, \mathbf{r}_3)$  represents the 9-dimensional configuration space of the particles and  $E_T$  is an energy offset used to control the walker population. As  $\tau \rightarrow \infty$ , the components of the trial wave function corresponding to excited states decay exponentially faster than the ground state,  $\Psi(\mathbf{R}, \tau)$  approaches the lowest-energy eigenstate consistent with the imposed symmetry.

To reduce variance, one uses importance sampling with a (real, positive) trial wave function  $\Psi_T(\mathbf{R})$  and propagates the mixed distribution  $f(\mathbf{R}, \tau) = \Psi_T(\mathbf{R})\Psi(\mathbf{R}, \tau)$ :

$$-\frac{\partial f}{\partial \tau} = -\frac{1}{2}\nabla_{\mathbf{R}}^2 f + \nabla_{\mathbf{R}} \cdot [\mathbf{v}_D(\mathbf{R})f] + (\mathcal{E}_L(\mathbf{R}) - \mathcal{E}_T) f, \quad (19)$$

where  $\nabla_{\mathbf{R}}$  is the gradient in the full configuration space,

$$\mathbf{v}_D(\mathbf{R}) = \nabla_{\mathbf{R}} \ln \Psi_T(\mathbf{R}) \quad (20)$$

is the drift velocity, and

$$\mathcal{E}_L(\mathbf{R}) = \frac{\hat{H}\Psi_T(\mathbf{R})}{\Psi_T(\mathbf{R})} \quad (21)$$

is the local energy. Equation (19) has the form of a drift–diffusion process with a branching term proportional to  $E_L - E_T$  [153, 181, 182].

In the DMC calculations, usually a Slater–Jastrow trial wave function was employed,

$$\Psi_T(\mathbf{R}) = \mathcal{A} \left\{ \chi_{\text{spin}}^S \left[ \prod_i \phi_i(\mathbf{r}_i) \right] \exp \left( \sum_{i < j} u(r_{ij}) \right) \right\}, \quad (22)$$

where  $\mathcal{A}$  enforces antisymmetry for identical fermions,  $\phi_i$  are single-particle orbitals, and  $u(r_{ij})$  is a two-body Jastrow correlation factor that satisfies the appropriate Coulomb cusp conditions.

In the context of TMDC, DMC has proven instrumental for determining the stability of complex many-body states. Studies [153, 181–184] utilize DMC to calculate the binding energies of excitonic complexes. These calculations typically involve a model Hamiltonian that accounts for the screened RK potential (1).

Trions binding energy are computed relative to dissociation into an exciton plus a free carrier by analogously as given in Eq. (17), where  $\mathcal{E}(X)$  and  $\mathcal{E}(X^\pm)$  are the total ground-state energies obtained from DMC for the exciton

and trion Hamiltonians, respectively [153, 181–184]. In addition to binding energies, DMC yields statistically exact pair-correlation functions and contact densities, which can be used to parameterize short-range exchange or contact interactions perturbatively [153, 182–184].

By employing DMC, one can bypass the limitations of variational methods and obtain high-accuracy results that account for the strong correlation between carriers in monolayer TMDCs [181]. Furthermore, this approach allows for the investigation of how the binding energy scales with the effective mass ratio and the dielectric environment [153, 183, 184], providing a benchmark for experimental photoluminescence data.

### *Path-integral Monte Carlo for 2D trions*

The path-integral Monte Carlo method provides a nonperturbative framework for treating strongly correlated few-body quantum systems as thermal systems at a finite temperature. The approach is based on the real-time path-integral formulation of the density matrix introduced by Feynman [185, 186]. Then the central idea is that the few-body system, which has no thermal properties, is translated *formally* into a grand-canonical ensemble at a non-zero temperature  $T$  by an analytic continuation of the real time  $t$  to the imaginary time  $-it$ , also known as Wick rotation. The advantage of this translation is that the thermal system can be treated with standard techniques of Monte-Carlo integration. In contrast to diffusion DMC, which projects the ground-state wave function  $\Psi(\mathbf{R})$  in imaginary time, PIMC is formulated directly in terms of the finite-temperature density matrix and does not rely on a trial ground-state wave function.

A central quantity in PIMC is the canonical partition function

$$Z = \text{Tr} e^{-\beta \hat{H}}, \quad (23)$$

where  $\hat{H}$  is the trion Hamiltonian and  $\beta = 1/(k_B T)$ , with  $k_B$  denoting the Boltzmann constant and  $T$  the temperature. In coordinate representation, the trace is expressed as

$$Z = \int d\mathbf{R} \langle \mathbf{R} | e^{-\beta \hat{H}} | \mathbf{R} \rangle, \quad (24)$$

where  $\mathbf{R} = (\mathbf{r}_1, \mathbf{r}_2, \mathbf{r}_3)$  denotes the set of particle coordinates.

To clarify the origin of the imaginary-time formulation used in PIMC, one may start from the real-time evolution operator describing the dynamics of the system over the time interval  $[0, t]$ ,

$$U(t) = e^{-i\hat{H}t/\hbar}. \quad (25)$$

Applying the Wick rotation  $t \rightarrow -i\beta\hbar$  transforms the real-time evolution into imaginary-time evolution, yielding the thermal distribution operator (Boltzmann density operator)  $e^{-\beta\hat{H}}$ , which appears in the partition function. To calculate  $Z$ , we use the Trotter decomposition [187, 188], in which the density matrix is factorized into  $M$  imaginary-time slices

$$e^{-\beta\hat{H}} = \lim_{M \rightarrow \infty} \left( e^{-\Delta\tau\hat{H}} \right)^M, \quad \Delta\tau = \beta/M. \quad (26)$$

For a finite  $M$  we can write the product of operators  $e^{-\Delta\tau\hat{H}}$  in coordinate representation  $\langle \mathbf{R} | e^{-\Delta\tau\hat{H}} | \mathbf{R}' \rangle$ . After inserting this matrix product into  $Z$  we get the path integral

$$Z = \lim_{M \rightarrow \infty} \int \prod_{k=1}^M d\mathbf{R}_k \exp \left[ - \sum_{k=1}^M \left( \frac{m}{2\hbar^2\Delta\tau} |\mathbf{R}_k - \mathbf{R}_{k+1}|^2 + \Delta\tau V(\mathbf{R}_k) \right) \right]. \quad (27)$$

This mapping transforms the quantum problem into an equivalent classical system of three interacting ring polymers, each consisting of  $M$  imaginary-time beads connected by harmonic springs arising from the kinetic-energy contribution.

In a general treatment of three charged fermions of different masses, the constituting particles of the trion can be treated as distinguishable, and exchange permutations are therefore neglected. Thus, the partition function is written in the Boltzmann form without antisymmetrization of the density matrix. The absence of permutation operators indicates that exchange effects between identical particles are ignored, while the quantum nature of the particles is still fully retained through the path-integral formulation. Corresponding expressions for fermionic PIMC can be found in Ref. [189], where permutations between identical particles are explicitly included.

PIMC has been applied extensively to excitonic complexes in two-dimensional semiconductors, including excitons, trions, and biexcitons, where it captures strong Coulomb correlations and finite-temperature effects. Representative applications to monolayer transition-metal dichalcogenides and related systems include Refs. [190, 191]. PIMC also applied to excitonic complexes in quantum wells. Filinov, Bonitz, and Lozovik [192] performed one of the first first-principles path-integral Monte Carlo studies of strongly correlated excitonic complexes—including excitons, trions, and biexcitons—in semiconductor quantum wells, obtaining accurate binding energies and correlation properties as functions of quantum-well width.

Thermodynamic observables, such as the internal energy and pair-correlation functions, are obtained as ensemble averages over these imaginary-time paths. PIMC has been extensively applied to excitons, trions, and biexcitons in quantum dots, see, for example application for trions in quantum dots [193], where it accurately captures strong Coulomb correlations and finite-temperature effects. Later works used improved PIMC algorithms to treat larger electron clusters in quantum dots and analyze Wigner-molecule formation and correlation effects [194].

Authors [195] report binding energies of trions and provide a direct, head-to-head comparison between the SVM and PIMC results. The authors demonstrated that at the zero-temperature limit,  $T \rightarrow 0$ , the results of the PIMC calculations converge with the SVM results. This was a critical "sanity check" for the community, proving that both stochastic wavefunction optimization within the SVM framework and stochastic sampling of the density matrix within PIMC yield the same binding energies for trions and biexcitons. Additionally, the combined density functional theory and PIMC study by Kylänpää and Komsa [190] provides further PIMC binding-energy results for exciton complexes.

Unlike variational approaches, PIMC does not require an explicit trial wave function and is therefore free of variational bias. However, for fermionic systems it suffers from the fermion sign problem, which results from the antisymmetrization of the density matrix and limits simulations to small particle numbers or moderate temperatures. Despite this limitation, PIMC provides an important benchmark for zero-temperature variational and diffusion Monte Carlo methods and plays a central role in validating theoretical descriptions of excitonic complexes in two-dimensional semiconductors.

DMC calculations of Mott–Wannier trions in 2D systems have been carried out primarily for monolayer TMDC and idealized 2D models, Refs. [153, 181, 182, 184], as well as for indirect trions in coupled quantum wells modelled by two-dimensional bilayers Ref. [196].

### C. Faddeev equations approach for trions

Because trions are intrinsically three-body systems, their theoretical description requires a genuine three-body treatment beyond effective two-body models. In particular, the pairwise nature of interactions and the mass asymmetry between electrons and holes prevents an exact separation into independent subsystems. A natural and rigorous framework for addressing such problems is provided by the Faddeev equations, which allow the systematic decomposition of the total three-body wave function into components associated with pairwise interactions.

Within the Faddeev formalism, the total trion wave function  $\Psi$  can be expressed in terms of Faddeev components  $\psi_{ij}$  as:

$$\Psi = \sum_{i < j}^3 \psi_{ij}. \quad (28)$$

The component  $\psi_{ij}$  corresponds to a specific interacting pair  $(ij)$ , with  $i \neq j \neq k = 1, 2, 3$ . Each Faddeev component satisfies an integral [197, 198] or differential [199, 200] equation that explicitly accounts for the interaction within the selected pair while incorporating the influence of the third particle through coupling to the remaining components. The number of Faddeev components  $\psi_{ij}$  equals the number of distinct binary interactions. These equations constitute a set of three Faddeev equations for a three-body problem, read

$$\psi_{ij} = (\mathcal{E} - \hat{H}_0)^{-1} \hat{V}_{ij} \Psi, \quad (29)$$

where  $\hat{H}_0 = -\sum_{i=1}^3 \frac{\hbar^2}{2m_i} \nabla_i^2$  is the Hamiltonian of three non-interacting particles and  $\hat{V}_{ij}$  denotes the interaction between particles  $i$  and  $j$ .

The advantage of the Faddeev approach lies in its ability to treat all pairwise interactions on an equal footing and to properly account for correlation effects that are essential for binding in three-body systems. In particular, it avoids double counting of interaction terms and ensures the correct asymptotic behavior of the wave function. This makes the formalism especially suitable for studying trion binding energies and structural properties in low-dimensional systems, where correlation effects are enhanced.

In practical applications to semiconductor trions, the Faddeev equations may be formulated either in configuration space or in momentum space, depending on the choice of interaction potential and numerical strategy. In bulk materials, configuration-space differential Faddeev equations with Coulomb interactions were first successfully employed to study trions in Refs. [14, 201].

In contrast, Ref. [202] developed a momentum-space Faddeev formalism to investigate trions in semiconductor layered materials, treating three charged particles confined to two dimensions. In that work, the authors solved the coupled Faddeev integral equations in momentum space for both a short-range separable Yamaguchi potential and the long-range Rytova–Keldysh interaction, with applications to trions in a MoS<sub>2</sub> monolayer.

For trions, symmetry considerations play a crucial role. In the case of identical effective masses for electrons or holes, a negative trion  $X^-$ , consisting of two identical electrons and one hole, the total wave function must be antisymmetric under exchange of the two electrons. This constraint reduces the number of independent Faddeev components and leads to a coupled set of two differential equations [203–208] with well-defined symmetry properties. An analogous consideration applies to positive trions  $X^+$ , where the two holes are identical fermions.

The Faddeev framework thus provides a rigorous theoretical foundation for the description of trions, complementing variational, hyperspherical, and quantum Monte Carlo approaches, and offering valuable insight into the role of three-body correlations in excitonic complexes.

#### D. Hyperspherical harmonics formalism

The hyperspherical harmonics (HH) method was first introduced for the description of charged excitons in quantum wells [22, 209] and subsequently applied to trions in quantum dots using either the standard HH expansion [210] or correlated HH expansions [211, 212], the latter being employed to accelerate convergence in Coulomb-interacting three-particle systems in quantum dots. A comprehensive exposition of the HH method is provided in Refs. [213–215].

The SVM with explicitly correlated Gaussian basis functions has been employed to obtain highly accurate few-body solutions for excitonic complexes such as excitons, trions, and biexcitons confined in semiconductor quantum dots within the effective-mass approximation. Complementary to this approach, trion calculations in quantum dots using the HH method are typically formulated as a three-dimensional three-body problem with external parabolic confinement [216]. In this formulation, the HH expansion is performed in the six-dimensional configuration space, and the Coulomb interaction retains its three-dimensional form, while quasi-two-dimensional effects are incorporated through anisotropic confinement parameters. In Refs. [210, 217], the HH method was extended to describe two-dimensional trion, biexciton, and triexciton states confined in quantum dots under a magnetic field.

By contrast, the HH approach developed and applied for the first time in Refs. [143, 144, 201, 218, 219] treats trions in atomically thin two-dimensional materials as intrinsically 2D three-body systems. In this framework, the relative motion is described in a four-dimensional hyperspherical space, and the interparticle interaction is governed by the Rytova–Keldysh potential, which accounts for nonlocal dielectric screening in layered materials. As a result, the corresponding hyperradial equations differ qualitatively from those obtained in conventional three-dimensional formulations.

To solve the three-body Schrödinger equation (7) for a trion in a two-dimensional configuration space, the authors employ the method of hyperspherical harmonics. Within this framework, the relative motion of three particles interacting via centrally symmetric pairwise potentials, either the Rytova–Keldysh potential (1) or the modified Kratzer potential (2), is mapped onto the effective motion of a single particle in a four-dimensional (4D) hyperspace with a reduced mass  $\mu$ . Following Refs. [143, 144, 219], the solution of Eq. (7) is obtained by introducing hyperspherical coordinates in the four-dimensional configuration space. The hyperradius is defined as

$$\rho = \sqrt{x_i^2 + y_i^2}, \quad (30)$$

while the hyperangular variables are collected into  $\Omega_i = (\alpha_i, \varphi_{x_i}, \varphi_{y_i})$ , with  $x_i = \rho \cos \alpha_i$  and  $y_i = \rho \sin \alpha_i$ .

In hyperspherical coordinates, the Schrödinger equation takes the form

$$\left[ -\frac{\hbar^2}{2\mu} \left( \frac{\partial^2}{\partial \rho^2} + \frac{3}{\rho} \frac{\partial}{\partial \rho} - \frac{\hat{K}^2(\Omega_i)}{\rho^2} \right) + \sum_{j=1}^3 V(\rho \cos \alpha_j) - \mathcal{E} \right] \Psi(\rho, \Omega_i) = 0, \quad (31)$$

where  $\hat{K}^2(\Omega_i)$  is the grand angular momentum operator in four dimensions [213–215].

The wave function is expanded in the complete orthonormal basis of hyperspherical harmonics,

$$\Psi(\rho, \Omega_i) = \rho^{-3/2} \sum_{K\lambda} u_{K\lambda}(\rho) \mathcal{Y}_{K\lambda}^L(\Omega_i), \quad (32)$$

where  $K$  is the grand angular momentum,  $\lambda$  denotes the set of partial angular momenta, and  $\mathcal{Y}_{K\lambda}^L$  are eigenfunctions of  $\hat{K}^2$ :  $\hat{K}^2\mathcal{Y}_{K\lambda}^L = K(K+2)\mathcal{Y}_{K\lambda}^L$  [214, 215].

Substituting Eq. (32) into Eq. (31) and integrating over the hyperangular variables yields a system of coupled differential equations for the hyperradial functions,

$$\left[ \frac{d^2}{d\rho^2} - \frac{(K+1)^2 - \frac{1}{4}}{\rho^2} + \kappa^2 \right] u_{K\lambda}(\rho) = \frac{2\mu}{\hbar^2} \sum_{K'\lambda'} W_{K\lambda, K'\lambda'}(\rho) u_{K'\lambda'}(\rho), \quad (33)$$

where  $\kappa^2 = 2\mu B/\hbar^2$ , with  $B$  being the trion binding energy.

The effective coupling potential is given by

$$W_{K\lambda, K'\lambda'}(\rho) = \int \mathcal{Y}_{K\lambda}^{L*}(\Omega_i) \left[ \sum_{j=1}^3 V(\rho \cos \alpha_j) \right] \mathcal{Y}_{K'\lambda'}^L(\Omega_i) d\Omega_i. \quad (34)$$

The coupled system of equations (33) thus describes the motion of an effective particle in 4D configuration hyperspace in a centrally symmetric coupling field defined by Eq. (34).

To summarize, the HH method reformulates the three-body trion problem—two identical charge carriers and a distinguishable third—in terms of mass-scaled Jacobi coordinates and a single hyperradial coordinate, thereby mapping the two-dimensional three-body Schrödinger equation onto a coupled-channel problem in a four-dimensional hyperspace. The total wave function is expanded in a complete HH basis over the hyperangles, leading to a system of coupled hyperradial equations whose controlled truncation provides a systematic, nonperturbative treatment of three-body correlations. This approach proved effective for  $X^-$  and  $X^+$  trions in 2D materials, where the HH expansion captures correlation and symmetry effects beyond simple variational ansätze. In modern atomically thin semiconductors, the HH formalism has been adapted to include physically realistic screened interactions, such as the Rytova–Keldysh potential, and has been successfully applied to compute trion binding energies and systematic trends across TMDC [201, 218, 219] and buckled Xenes, including their tunability under external electric field [143, 144].

Although excitonic systems are inherently many-body in nature, they can be effectively treated within few-body frameworks [220]. The Faddeev equations and the hyperspherical harmonics method, originally developed in nuclear and atomic physics, have been adapted to two-dimensional three-body systems calculations in Refs. [202, 210, 221, 222].

## VII. BENCHMARKING AND SPECTRAL COMPLEXITY OF TRIONS IN 2D MONOLAYERS

Trions play a central role in the valley dynamics of emerging 2D semiconductors. In monolayers, trion properties are governed by coupled spin and valley degrees of freedom. The absence of inversion symmetry, together with strong spin–orbit coupling, leads to a large valence-band splitting in monolayer TMDCs [151]. This splitting removes the spin degeneracy of electron and hole states in the  $K$  and  $K'$  valleys, allowing excitation of carriers with distinct spin–valley configurations. The valley degree of freedom has been extensively investigated in molybdenum- and tungsten-based dichalcogenide monolayers using helicity-resolved photoluminescence, time-resolved photoluminescence, reflectance spectroscopy, and the time-resolved Kerr rotation technique [72, 108, 109, 113, 223–231].

The absolute minima of the conduction band and the absolute maxima of the valence band in TMDC monolayers are located at the two non-equivalent hexagonal Brillouin-zone corners,  $K$  and  $K'$ . The lack of inversion symmetry combined with spin–orbit interaction results in coupled spin and valley degrees of freedom, such that the circular polarization of absorbed or emitted photons is directly linked to a specific valley,  $K$  or  $K'$  [151, 225]. These valley-contrasting optical selection rules enable selective excitation and manipulation of the valley index. Experimental studies [72, 223] demonstrate that each valley can be selectively excited by light of a given helicity. With the additional valley index  $\tau$  alongside spin, one distinguishes between two types of trions: intravalley and intervalley. For intravalley trions  $\tau_1 = \tau_2$ , while for intervalley trions  $\tau_1 \neq \tau_2$ .

A symmetry analysis of the different  $X^-$  and  $X^+$  trion states, classified by the valley configurations as well as the spin configuration, is performed [119, 219, 232–234]. Depending on the spin configuration of the electron–hole pairs, intravalley excitons of TMDC monolayers can be either optically bright or dark. These analyses [119, 219, 231, 232, 234] show that the negative and positive trions can be optically bright or dark, as illustrated in Fig. 4. Experimental studies [121, 235] have revealed evidence of dark trions in monolayer WSe<sub>2</sub> under a strong in-plane magnetic field.

The structural and spin-valley complexity of TMDC monolayers leads to rich energetic properties [118, 119, 237–239]. The  $K$  and  $K'$  valleys, separated in momentum space, together with strong spin-orbit coupling, give rise to singlet and triplet trion configurations [238]. A hybrid parameter-free theory, combining configuration interaction and Green's function approaches, was proposed to study charged excitations [240]. This fully first-principles many-body

framework, based on the GW–Bethe–Salpeter approach, allows for the investigation of neutral excitons and charged trions in monolayer TMDCs. The authors computed trion fine-structure splittings arising from exchange interactions and spin–valley coupling, providing quantitative predictions for singlet–triplet energy separations and clarifying the microscopic origin of trion fine structure beyond traditional effective-mass models.

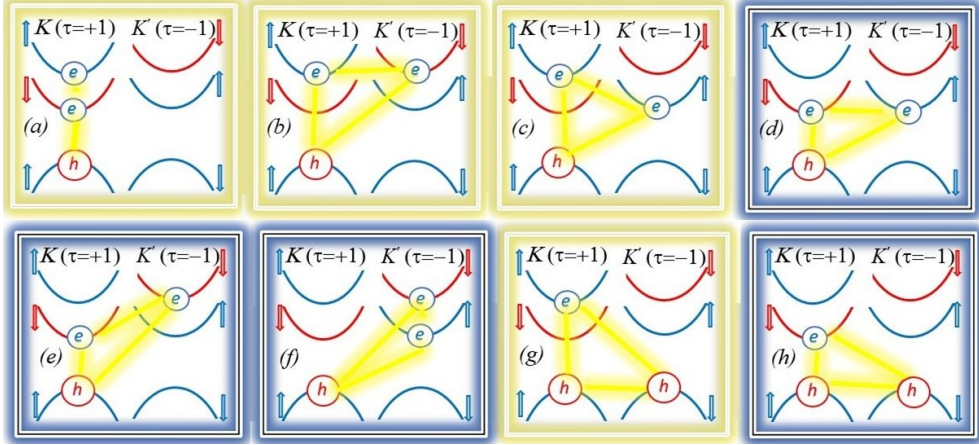


FIG. 4. (Color online) Schematic illustration of WSe<sub>2</sub> low-energy band structure and the spin-valley configurations of the constituent charge carriers. The topmost spin-subband for the valence band and the lower and upper spin-orbit split conduction band are shown. Arrows denote bands with up (down) spin. The hole has the opposite spin of the valence electron [236]. Light and dark rectangles indicate the bright and dark trions, respectively. (a), (b), (c), (d), and (e) correspond to  $X^-$  trions. (g) and (h) correspond to  $X^+$  trions. The bright trions emit circularly polarized light in the out-of-monolayer plane direction, while the dark trions emit vertically polarized light in the in-monolayer plane direction [121]. Lines indicate interaction between three charged particles. The remaining configurations are the time reversal of those shown in the figure. Adapted from Ref. [219].

Negative trions can be optically bright or dark depending on the spin configuration of their constituent electron–hole pair: radiative recombination occurs when the electron and hole spins are aligned, whereas spin mismatch—typically involving the lower spin–orbit–split conduction band—suppresses emission, leading to dark trions; such dark trion states were theoretically predicted in Refs. [241, 242]. The intravalley  $X^-$  trion exists in a spin-singlet state, whereas the intervalley  $X^-$  trion can form spin-singlet or spin-triplet states. Consequently, these excitonic complexes can manifest as either spin-forbidden or momentum-forbidden dark states. An intriguing feature is that in cross-circularly polarized experiments, trions created in the  $K$  valley in the singlet state (Fig. 4a) are converted to intervalley singlet trions with an electron in the  $K'$  valley (Fig. 4c) via spin flip and electron–hole exchange interaction [117].

In contrast to  $X^-$ , the positive trion  $X^+$  consists of two holes occupying the topmost valence subbands in the  $K$  and  $K'$  valleys and an unpaired electron in one of the conduction subbands; by the Pauli exclusion principle, it can exist only in the intervalley configuration. The  $X^+$  trion is optically bright when the electron and hole spins are aligned (Fig. 4g) and dark otherwise (Fig. 4h).

Now let’s start the comparison of the results obtained in different theoretical and computational approaches. The theoretical investigation of trion binding energies in monolayer TMDCs reveals a dependence on material properties, the input parameters such as electron and hole effective mass, the screening distance chosen within the computational methodology, and the underlying physical approximations. Table II highlights a general consensus across diverse theoretical frameworks regarding the magnitude of these energies, typically falling within the range of 20 to 35 meV for common TMDCs such as MoS<sub>2</sub>, MoSe<sub>2</sub>, WS<sub>2</sub>, and WSe<sub>2</sub>. This overall agreement suggests that, despite methodological differences, the effective-mass framework combined with screened Coulomb interactions provides a reliable description of trion binding in these systems.

Deterministic few-body approaches, such as the variational method and exact diagonalization, provide foundational estimates. Early variational work by Berkelbach et al. [156] established binding energies near 26 meV for WS<sub>2</sub>, while more recent high-precision ED calculations [166] report values around 32.6 meV. The SVM [162], known for its high accuracy in few-body problems, yields slightly higher values, such as 33.8 meV for WS<sub>2</sub>. The GEM [173] shows excellent agreement with the SVM [162]. This progression in values highlights how refined computational treatments of electron-hole correlations and non-local screening can lead to more robust predictions of trion binding.

Both DMC and PIMC provide numerically exact benchmarks that do not rely on a specific wavefunction ansatz. DMC results show a high degree of agreement with SVM. PIMC values are lower, illustrating the subtle differences in how stochastic methods handle the complex many-body interactions in these 2D systems.

The use of Faddeev equations and the hyperspherical harmonics method provides a rigorous treatment of the

TABLE II. Comparison of  $X^-$  trion binding energies in representative TMDC monolayers. Results are compiled from various theoretical frameworks, each utilizing specific sets of electron and hole effective masses and dielectric screening lengths as input parameters. Values are provided in meV.

Method	MoS <sub>2</sub>	MoSe <sub>2</sub>	WS <sub>2</sub>	WSe <sub>2</sub>	Reference
<i>Deterministic Few-Body Approach</i>					
VM	26	21	26	22	[156]
	31.6	27.7	32.4	28.3	[157]
SVM	33.7	28.2	33.8	29.5	[162]
ED	31.82	27.84	32.60	28.55	[166]
	31.7	27.7	34.2	28.4	[165]
GEM	33.7	28.2	33.8	29.5	[173]
<i>Quantum Monte Carlo Approach</i>					
DMC	33.8	28.4	34.0	29.5	[181]
PIMC	32.0	27.7	33.1	28.5	[190]
<i>Faddeev Equations</i>					
FE	49.6	—	—	—	[202]
<i>Hyperspherical Harmonics</i>					
HH	32.8	27.6	33.1	28.3	[201, 219]

three-body problem, approaches that are well established in nuclear physics. While HH results align well with other methods, the Faddeev approach has produced significantly higher outliers, such as 49.6 meV, suggesting a higher sensitivity to the choice of potential and basis set in that specific framework.

An analysis of the material-specific trends summarized in Table II consistently indicates that sulfur-based TMDCs exhibit higher trion binding energies than their selenium-based counterparts. For instance, across nearly all methods, the binding energy for MoS<sub>2</sub> is roughly 4-5 meV greater than for MoSe<sub>2</sub>. This trend is primarily attributed to the smaller effective masses and different dielectric screening properties associated with selenium, which reduce the overall Coulombic attraction between the constituent carriers.

To conclude, the robustness of these binding energies—which are significantly larger than those found in traditional 3D semiconductors—is a direct consequence of the reduced dimensionality and non-local dielectric screening characteristic of 2D materials. The strong agreement between independent methods like DMC, SVM, ED, GEM, and HH reinforces the validity of the effective-mass model when combined with an appropriate interaction potential, such as the Rytova-Keldysh potential, to describe charged excitonic complexes in the monolayer limit.

Many studies have been devoted to calculating the binding energies and wave functions of excitonic complexes in monolayer TMDCs (see reviews [220, 232, 243–245]). Theoretical investigations of negatively and positively charged trions,  $X^-$  and  $X^+$ , have employed a broad spectrum of analytical and numerical techniques yielding binding energies in good agreement with experimental observations.

Beyond the deterministic [156, 157, 162–166, 173] and quantum Monte Carlo [153, 181, 182, 184, 190, 191, 246] approaches, extensive theoretical studies have utilized complementary techniques. These include effective-mass three-body models with nonlocal dielectric screening, first-principles many-body approaches (GW/BSE and configuration interaction), time-dependent density-matrix functional theory, and exciton–polaron formalisms that incorporate many-body interactions with the Fermi sea, and others.

The stochastic variational method with correlated Gaussian bases [162–164] has been widely applied to investigate trion binding energies and their dependence on screening length and effective mass ratios. Extensions of this approach include the influence of external magnetic fields and phonon recombination processes [247], as well as the study of narrow resonance states using complex scaling and stabilization techniques.

In Ref. [103] authors developed a many-body theory for 2D semiconductors that describes trion absorption features as Fermi polarons, treating the trion not as an isolated three-body bound state but as a collective interaction between an exciton and the surrounding Fermi sea of electrons.

The theoretical description of trionic excitations has evolved from first-principles density frameworks to collective many-body models. In Ref. [248] the authors utilized time-dependent density-matrix functional theory (TDDMFT) to treat trions as discrete three-body excitations. By incorporating a three-body kernel into the density-matrix equations of motion, this approach provides a rigorous microscopic derivation of the trion’s internal structure and its role in the nonlinear optical response of monolayers like MoS<sub>2</sub>.

In contrast, Efimkin and MacDonald [103] introduced a many-body framework that reinterprets trion absorption features as Fermi polarons. In this picture, the trion is not viewed as an isolated bound state, but as an exciton “dressed” by its interactions with the surrounding resident carrier sea, described via a  $T$ -matrix scattering formal-

TABLE III. Trion binding energies for representative 2D semiconductors, including TMDC monolayers and phosphorene, under different dielectric environments: suspended, on a hBN substrate, and encapsulated by hBN. Energies are given in meV.

Material	Suspended	On substrate	Encapsulated
MoS <sub>2</sub>	32.12	21.59	15.83
MoSe <sub>2</sub>	32.00	22.60	17.18
WS <sub>2</sub>	34.49	23.60	15.94
WSe <sub>2</sub>	33.15	21.93	16.14
Phosphorene	51.77	32.65	22.82

ism. While the TDDMFT approach captures the specific quantum-mechanical bonds of the three-particle complex, the polaron model provides a more accurate description of the asymmetric spectral line shapes and the continuous evolution of quasiparticle energy levels as a function of carrier density.

Within the effective-mass framework, a microscopic description of trions in monolayer TMDCs was developed in Ref. [156], where the calculated binding energies were found to be in good agreement with many-body Bethe–Salpeter equation results. Building on this foundation, subsequent study introduced variational approaches based on two-dimensional Slater-type orbitals, which enabled efficient and accurate calculations of trion binding energies and wave functions [157].

Alternative formulations include mapping the three-body problem with logarithmic interactions to an effective one-particle problem treated with the boundary-matching-matrix method [233]. Trion states have also been computed via direct diagonalization of the three-particle Hamiltonian within the Tamm–Dancoff approximation [249, 250]. Both multi-band and single-band models have been explored using finite-element and stochastic variational methods [155, 162]. The electronic and structural properties of excitons and trions in monolayer transition metal dichalcogenides were investigated within both multiband and single-band models [155]. The energy eigenvalue equation was solved using the finite element method (FEM) as well as the SVM. While good agreement was found between the two approaches—and with other theoretical works—for excitons, the consistency for trions was less satisfactory. This discrepancy stems from the neglect of angular correlations in the FEM treatment, which are vital for describing complex three-body states.

Substrate screening, doping, and temperature effects further modify trion binding energies and fine-structure splitting [118, 234, 251]. Optical spectroscopy, including photoluminescence and reflectivity measurements, has played a central role in extracting trion binding energies and revealing differences between positive and negative trions [118, 119, 239, 252, 253]. Short-range Coulomb interactions and exchange effects have been proposed as mechanisms for fine-structure splitting in WSe<sub>2</sub> monolayers [119, 253, 254]. Substrate-induced screening and polarization are also known to reduce binding energies in supported structures [118].

The many-body nature of excitons and trions in doped 2D semiconductors, particularly TMDCs, has been extensively investigated in recent literature [255–257]. These studies highlight a fundamental crossover from isolated few-body trion states at low doping to an exciton-polaron regime at higher carrier densities. Using a composite-boson formalism, Ref. [255] demonstrated that excitons become dressed by Fermi sea excitations, with energy features shifting due to many-body screening and exchange. This was expanded by Chang and Reichman [256] via a diagrammatic  $T$ -matrix approach, which mapped doping-induced spectral shifts and broadening onto polaronic quasiparticle dynamics. Further, Rana et al. [257] employed linear-response theory and a coupled Schrödinger-like framework to model optical conductivity, showing how strong Coulomb correlations hybridize these states. Collectively, these studies establish that a purely few-body description is insufficient in doped 2D systems. Instead, a many-body framework is required to capture the continuous evolution from isolated trionic bound states to many-body dressed quasiparticle, thereby providing a unified theoretical basis for interpreting doping-dependent optical experiments in TMDC monolayers.

More recently, high-lying excitons and trions involving carriers with negative effective mass were investigated within a variational framework [258], demonstrating the crucial role of nonparabolic conduction band dispersion in stabilizing such bound states.

Studies on the temperature dependence of excitonic features in TMDCs reveal the critical role of phonon scattering and thermal distribution in quasiparticle stability. In Ref. [101] authors utilized temperature-dependent photoluminescence to demonstrate that in monolayer MoS<sub>2</sub>, the trion-to-exciton intensity ratio decreases with rising temperature due to the thermal dissociation of the three-body complex. More recently, Nguyen et al. (2024) [102] extended this analysis to WSe<sub>2</sub>, identifying that the redshift and broadening of both exciton and trion peaks follow the O’Donnell-Chen model [259], while emphasizing that the trion binding energy remains relatively robust against thermal fluctuations compared to the significant changes in non-radiative recombination rates.

Interestingly enough, in [260], authors demonstrated that trion-like features observed in the photoluminescence

of monolayer TMDCs can originate from virtual trion states formed through many-body exciton-carrier scattering processes, where Coulomb interactions with the Fermi sea dynamically dress the exciton and enable recombination through intermediate, non-fully bound three-body configurations rather than through stable trion states.

In the work by Cavalcante *et al.* [261], trion binding energies were theoretically studied for several two-dimensional materials, with particular emphasis on TMDCs and black phosphorus under an external electric field. The binding energies calculated in the absence of an electric field are summarized in Table III. The data clearly indicate that trion binding energies are strongly influenced by both intrinsic material parameters and the surrounding dielectric environment. Comparing different materials, phosphorene monolayer exhibits a significantly stronger binding energy when suspended than TMDC family, which ranges between approximately 32 and 35 meV. Moreover, the comparatively larger binding energies in phosphorene highlight the role of its strongly anisotropic effective masses and reduced dielectric screening, which significantly enhance Coulomb correlations relative to isotropic TMDC systems. Beyond material type, the environmental conditions impose a drastic influence on stability; as the dielectric screening increases from a suspended state to a substrate-supported and eventually a fully encapsulated configuration, the binding energies decrease monotonically. For all listed semiconductors, encapsulation in hBN approximately halves the binding energy relative to the suspended case—for example, the binding energy of WS<sub>2</sub> drops from 34.49 meV to 15.94 meV. This highlights that while trions are robustly bound in 2D systems, their precise energy levels and stability are highly tunable through dielectric engineering of the surrounding medium.

Although early studies of trions in phosphorene predicted extraordinarily large trion binding energies exceeding 100 meV based on effective-mass models [262], subsequent *ab initio* studies utilizing the Bethe-Salpeter Equation refined these values to approximately 70–90 meV [263]. Recent theoretical studies have provided a more refined understanding of trions in phosphorene, emphasizing the crucial role of anisotropy, dielectric screening, and many-body correlations. In Refs. [132, 133] demonstrated that trion binding energies in phosphorene are highly sensitive to the dielectric environment, with substrate-induced screening substantially reducing the effective binding energy compared to earlier estimates, yielding values on the order of  $\sim 70$  meV in screened few-layer configurations. In a complementary many-body treatment, in Ref. [133] the authors developed a theoretical framework for trions in two-dimensional nanostructures and applied it to phosphorene nanoflakes, showing that realistic dielectric modeling reconciles theoretical predictions with experimental observations. Furthermore, Zhong *et al.* [264] investigated electric-field effects in quasi-1D phosphorene nanostructures, demonstrating that external fields can enhance excitonic binding by increasing carrier localization, thereby offering an additional mechanism for tuning Coulomb correlations in anisotropic phosphorene systems.

Thus, advanced many-body calculations clarified the role of dielectric screening and band anisotropy, showing that the apparent magnitude of trion binding energies in monolayer black phosphorus depends sensitively on the reference energy and environmental screening [132, 133, 262, 263]. Together, these works establish phosphorene as a viable platform for stable trions, while highlighting the importance of anisotropy and dimensional crossover effects in determining their binding and optical properties. Transition metal trichalcogenides also represent quasi-one-dimensional van der Waals semiconductors with strong Coulomb interactions and reduced dielectric screening, which can support strongly bound excitonic complexes, including trions [265].

## VIII. TRIONS IN EXTERNAL ELECTRIC AND MAGNETIC FIELDS

The influence of external electric fields on trions in two-dimensional materials has attracted considerable attention due to the tunability of their optical response, internal structure, and binding energies. Existing studies can broadly be categorized into two main directions: (i) works that explicitly compute the electric-field dependence of trion binding energies within a microscopic three-body framework, and (ii) investigations that analyze field-induced shifts of optical transition energies (Stark effect) without directly evaluating modifications of the underlying binding energy.

The behavior of trions in 2D materials under external magnetic fields has revealed rich valley, spin, and many-body phenomena. Magnetic fields lift valley degeneracy, modify spin-valley coupling, and affect both optical transitions and the binding energies of charged excitonic complexes. These effects provide valuable insight into their internal structure and correlated dynamics of trions in reduced dimensionality.

### A. Trions in 2D Materials under External Electric Fields

Electric fields provide a means of tuning on both the internal structure and optical signatures of trions in two-dimensional materials. A systematic and rigorous theoretical treatment of excitons and trions under an applied electric field was developed by Cavalcante *et al.* [261]. To account for the influence of the electric field on trions, one must add to the trion Hamiltonian (3) the interaction term  $-\mathbf{d} \cdot \mathbf{E}$ , where  $\mathbf{d}$  is the dipole moment and  $\mathbf{E}$  is the

external electric field. Within the effective-mass approximation and a screened Coulomb interaction, the authors [261] computed the Stark response of both neutral and charged excitonic complexes in TMDCs and phosphorene, and analyzed the stability of trions as a function of field strength. Their results demonstrate that electric fields modify the internal structure of the three-body wave function, leading to a reduction of the binding energy beyond a critical field.

More generally, the energy shift of an excitonic complex with  $s$ -state symmetry in an electric field  $\mathbf{E}$  can be expanded as [261]

$$\mathcal{E}(E) = \mathcal{E} + \frac{1}{2}\alpha E^2 + \frac{1}{24}\gamma E^4, \quad (35)$$

where  $\alpha$  and  $\gamma$  are the polarizability and hyperpolarizability, respectively. In monolayer TMDCs, intralayer trions typically exhibit a quadratic Stark effect, whereas in bilayer or layer-hybridized systems a linear contribution may arise due to a finite dipole moment.

Figure 5a illustrates the dependence of the trion binding energy in MoS<sub>2</sub> on an applied in-plane electric field due to the Stark effect. As the electric field strength increases, the trion binding energy decreases. The trion, consisting of three Coulomb-correlated charge carriers confined to a 2D sheet, becomes polarized under the applied field. This leads to a spatial separation of the electron and hole probability densities, which modifies the internal structure of the three-body wave function and shifts the trion energy relative to its zero-field value. Moreover, Fig. 5a demonstrates the robustness of the trion state: no dissociation occurs even for fields up to 60 kV/cm, as evidenced by the wave function projections in Fig. 5b for the suspended MoS<sub>2</sub> case. In the absence of an electric field (top row of Fig. 5b), both the excitonic and trionic components of the wave function are circularly symmetric. The trionic component exhibits a minimum at  $r = 0$  due to electron-electron repulsion. The applied in-plane electric field induces deformation of these distributions (bottom row of Fig. 5b), but they remain concentrated around the origin, indicating the absence of trion dissociation.

Trion binding energies depend on the dielectric environment (suspended, on-substrate, or encapsulated), but they remain sufficiently large to ensure stability under relatively strong electric fields, as shown in Fig. 5a MoS<sub>2</sub> case. Trions in phosphorene are particularly robust against applied fields, owing to the material's anisotropic effective masses and reduced dielectric screening. In monolayer phosphorene, for fields applied along the zigzag direction, even strengths as high as 100 kV/cm produce negligible shifts in binding energy (on the order of  $\sim 1$  meV or less) and virtually no change in the wave function distribution [261].

This robustness supports the potential for using in-plane electric fields to drive charged excitons across the material plane without dissociation, which could enable novel optoelectronic applications such as energy transfer via trion transport.

In parallel with theoretical studies, several experiments and theory–experiment collaborations focus on field-tunable trion transition energies. Electrically tunable trion resonances have been observed experimentally in several systems. For example, Ross *et al.* [266] demonstrated gate-controlled conversion between neutral and charged excitons in monolayer TMDCs. In Ref. [267], the authors reported gate-tunable dark trions in monolayer WSe<sub>2</sub>. More recently,

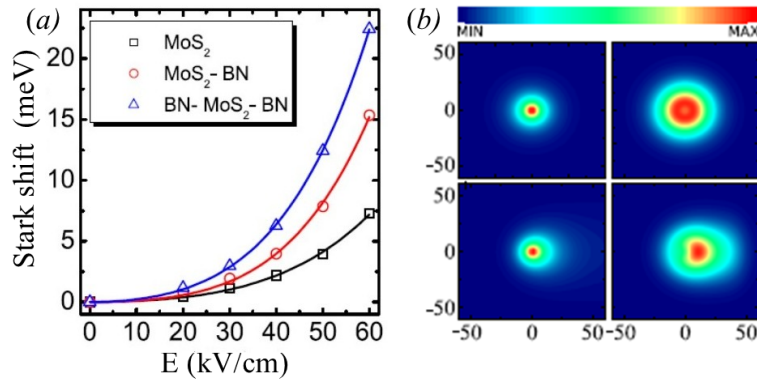


FIG. 5. (a) Numerically obtained field dependence of the trion binding energy in monolayer MoS<sub>2</sub> in the freestanding case, on a hBN substrate, and encapsulated by hBN. The values of polarizability and hyperpolarizability (fitting parameters for the curves) are presented in Ref [261]. (b) Contour map of the square modulus of the trion wave function in freestanding MoS<sub>2</sub>. The left (right) column represents the exciton's (trion's) center of mass wave function in the absence of the electric field in the first row, and for a  $E = 60$  kV/cm field applied in the  $x$  direction in the second row. The color scale goes from 0 (blue, MIN) to 0.012 (red, MAX). Adapted from [261].

Perea-Causin *et al.* [268] showed that an out-of-plane electric field in WSe<sub>2</sub> bilayers enables electrical control of layer-hybridized trion states and induces pronounced Stark red-shifts in photoluminescence spectra.

These studies collectively demonstrate that electric fields provide a powerful external knob for engineering trion stability, fine structure, and optical response in 2D materials.

Let us consider trions in Xenes under an applied perpendicular electric field. In Ref. [143], we demonstrated within the HH approach that perpendicular electric fields in Xenes act as a direct control parameter of the three-body Hamiltonian itself. In buckled 2D materials, an electric field creates an asymmetry between the two sublattices. This modifies the band gap and, consequently, the effective masses and the strength of Coulomb interactions between the constituent particles of the trion. Unlike conventional Stark-effect studies, where the field primarily induces polarization of the excitonic complex, in Xenes, the applied field simultaneously modifies the effective mass and dielectric screening, leading to a strong and nonperturbative tuning of trion binding energies. This behavior originates from a qualitatively different physical mechanism that operates in Xenes, where a perpendicular electric field  $E_{\perp}$  does not merely induce a Stark polarization of the trion wave function, but instead directly modifies the underlying single-particle band structure due to the intrinsic buckled lattice geometry. In these materials, the two sublattices are vertically displaced by a distance  $2l$ , where  $l$  is half the buckling constant, so that the application of  $E_{\perp}$  produces an electrostatic potential difference between sublattices. As a result, the field-dependent band gap takes the form [269]

$$\Delta_{\xi\sigma}(E_{\perp}) = |\Delta_{\text{SO}} \xi\sigma - eE_{\perp}l|, \quad (36)$$

where  $\Delta_{\text{SO}}$  is the intrinsic spin-orbit coupling,  $\xi = \pm 1$  denotes the valley index,  $\sigma = \pm 1$  the spin index,  $e$  is the elementary charge, and  $l$  is half the buckling height.

The effective mass therefore, becomes field dependent,

$$m^*(E_{\perp}) = \frac{\Delta_{\xi\sigma}(E_{\perp})}{2v_F^2}, \quad (37)$$

with  $v_F$  the Fermi velocity. Since the trion binding energy in a two-dimensional system approximately scales as

$$\mathcal{E}_b \sim \frac{\mu(E_{\perp})}{\varepsilon^2(E_{\perp})}, \quad (38)$$

where  $\mu(E_{\perp})$  is the reduced mass and  $\varepsilon(E_{\perp})$  the effective dielectric screening, the perpendicular electric field renormalizes the parameters of the few-body Hamiltonian rather than simply perturbing the three-body wave function.

This mechanism is fundamentally distinct from the conventional Stark effect in TMDC monolayers, where the band structure is essentially fixed and the electric field primarily induces polarization of the correlated excitonic complex. In Xenes, by contrast,  $E_{\perp}$  tunes the band gap continuously and can drive the system through regimes of enhanced or reduced effective mass, thereby significantly strengthening or weakening Coulomb correlations.

Consequently, the trion binding energy may exhibit a non-monotonic dependence on the applied field. Near the critical field at which the band gap closes ( $eE_{\perp}l \approx \Delta_{\text{SO}}$ ), the effective mass becomes small and screening effects are strongly modified, leading to substantial changes in the stability of excitonic complexes. In certain regimes, field-induced enhancement of binding is possible, while in others, increased screening or mass reduction suppresses the trion stability.

Thus, in Xenes the perpendicular electric field serves as a direct control parameter of the few-body Hamiltonian itself. This provides a unique platform for electrically tunable many-body physics, enabling controlled manipulation of trion binding energies, valley-spin selectivity, and potentially field-driven excitonic phase transitions.

At nonzero electric fields, both the valence and conduction bands split into upper subbands with a large gap (for  $\xi = -\sigma$ ) and lower subbands with a small gap (for  $\xi = \sigma$ ). We refer to excitons formed from charge carriers in the large-gap subbands as *A* excitons, and those formed from carriers in the small-gap subbands as *B* excitons. The external electric field affects the reduced masses of the *A* and *B* excitons differently, primarily due to their distinct intrinsic band gaps. The direct bright *A* and *B* excitons consist of electrons and holes with parallel spins. In all spin-valley configurations, the mass of the *A* exciton exceeds that of the *B* exciton.

The intravalley  $X^-$  and  $X^+$  trions exist only in the spin-singlet state, whereas intervalley trions can form either singlet or triplet states. Figures 6*d* and 6*e* present the binding energies of intravalley trions formed by an *A* exciton coupled to an electron in freestanding (FS), SiO<sub>2</sub>-supported, and hBN-encapsulated Xenes monolayers. A comparison of the binding energies (BEs) shows that FS monolayers exhibit significantly larger BEs due to the much weaker dielectric screening of the Coulomb interaction. The binding energy decreases for Xenes supported on SiO<sub>2</sub> and

is smallest for hBN-encapsulated structures, demonstrating the strong sensitivity of trion binding to the dielectric environment.

Intervalley singlet trions exhibit a qualitatively similar dependence on the external electric field as intravalley trions. In contrast, intervalley triplet trions in FS silicene and germanene monolayers have binding energies approximately three times smaller than those of the corresponding singlet states [143]. Moreover, both intra- and intervalley trions formed by a  $B$  exciton coupled to an electron possess smaller binding energies than those formed by an  $A$  exciton, since in all spin-valley configurations the mass of the  $A$  exciton exceeds that of the  $B$  exciton [143].

Figure 6f shows the probability distribution of the three particles forming an intravalley trion in a silicene monolayer. The corresponding distribution for intervalley trions differs slightly, with the difference arising from the distinct three-particle effective masses of intra- and intervalley trions [143]. An analysis of the probability distribution as a function of the hyperradius  $\rho$  and the external electric field indicates that increasing the electric field enhances the trion binding energy and leads to a more compact spatial structure. The stronger binding therefore, increases the probability of trion formation.

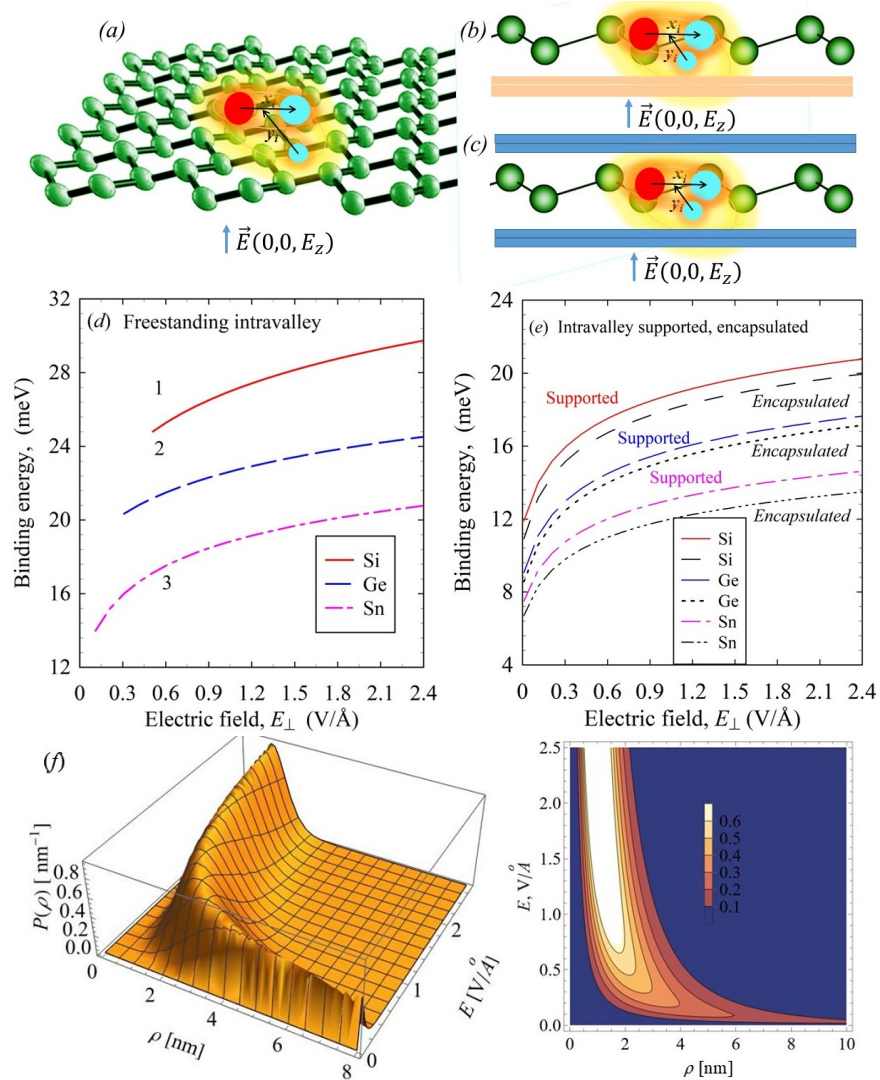


FIG. 6. Schematic representation of the  $X^-$  trion in the external electric field perpendicular to the Xene layer in (a) freestanding, (b) supported and (c) encapsulated Xenenes monolayer.  $x_i$  and  $y_i$  are Jacobi coordinates for the partition  $i$ . Dependencies of the binding energy of intravalley singlet state trions in silicene, germanene, and stanene on the applied electric field. (d) Curves 1, 2, and 3 correspond to the  $X^-$  trions formed by  $A$  excitons coupling an electron. The curves for freestanding Xenenes are truncated for the external electric field  $E_\perp$  less than a critical field. (e) The curves correspond to  $X^-$  trions in Xene monolayer supported on an SiO<sub>2</sub> substrate and hBN encapsulated. (f) Dependence of the probability distribution of three particles in freestanding silicene on hyperradius  $\rho$  and applied electric field for intravalley trion. Adapted from [143].

In many Xenes configurations, the effective masses of electrons and holes are not perfectly symmetric. As a result,  $X^+$  and  $X^-$  trions exhibit distinct binding-energy profiles under the same external electric field [143].

### B. Trions in 2D Materials under External Magnetic Field

The existence of tightly bound trions in monolayer TMDCs was first established experimentally by Mak *et al.* [92], who demonstrated gate-controlled formation of charged excitons in monolayer MoS<sub>2</sub>. Subsequently, magnetophotoluminescence measurements have demonstrated pronounced Zeeman splitting of trion resonances in monolayer TMDCs. In a single issue of *Nature Physics*, two seminal papers were published [270, 271] that provided the first direct experimental evidence of how a magnetic field breaks the "valley degeneracy" in monolayer WSe<sub>2</sub>. Together, these works established the definitive experimental foundation for the valley Zeeman effect in TMDCs. Aivazian *et al.* [271] demonstrated magnetic control of the valley pseudospin in WSe<sub>2</sub>, highlighting the distinct magnetic responses of neutral and charged excitons. Similarly, Mitioglu *et al.* [272] performed high-field optical studies of WSe<sub>2</sub>, resolving field-dependent exciton and trion transitions, further clarifying the diamagnetic shifts and  $g$ -factors of these complexes. Lyons *et al.* [273] expanded this scope by investigating the valley Zeeman effect in inter- and intravalley trions, demonstrating different  $g$ -factors for various charged excitonic species. Magnetically tunable dark trions were identified by Liu *et al.* [274], where the magnetic field enabled the separation of bright and dark charged complexes via their characteristic Zeeman splittings. In Ref. [275] experimentally investigated three-particle electron-hole complexes in high-mobility 2D electron systems under strong magnetic fields, revealing the formation and optical signatures of bound and metastable charged exciton states. Their results clarified the interplay between Coulomb interactions, Landau-level structure, and many-body effects in magneto-trion spectra. Kapuściński *et al.* [276] experimentally studied singlet and triplet trions in a WS<sub>2</sub> monolayer under an external magnetic field, showing that the valley Zeeman effect modifies the energies and relative intensities of trion states in polarization-resolved optical spectra.

On the theoretical side, variational calculations of singlet and triplet states of  $X^-$  and  $X^+$  trions confined in semiconductor quantum wells under a perpendicular magnetic field within the effective-mass approximation were carried out in Refs. [277, 278]. These studies analyzed how the trion binding energies, energy spectra, and correlation properties depend on the quantum-well width and magnetic-field strength, predicting singlet-triplet transitions and demonstrating good agreement with experimental observations in GaAs/AlGaAs quantum wells. *Ab-initio* many-body calculations [241, 279] showed the role of dark excitons and trions, whose energies and optical activity can be modified by magnetic fields and spin-orbit coupling. Complementary to these approaches, Ref. [280] developed a semi-analytical method providing universal estimates of trion binding energies. Further advancing these treatments, Ref. [281] performed detailed studies incorporating Landau-level (LL) structure and many-body correlations. Together, these works established the theoretical foundation of magnetotriion physics in conventional quasi-two-dimensional semiconductor systems.

The emergence of atomically thin TMDC monolayers introduced a new regime characterized by strong Coulomb interactions, reduced dielectric screening, and valley degrees of freedom. In contrast to GaAs-based structures, TMDC monolayers exhibit non-hydrogenic screening and pronounced spin-valley coupling, requiring modified theoretical frameworks. This shift has motivated renewed efforts to treat *c.m.*-internal coupling and Landau-level mixing in strictly two-dimensional materials.

In Ref. [247], the authors systematically investigated excitons, trions, and biexcitons in TMDC monolayers. Within an effective-mass framework, binding energies were computed using the stochastic variational method, demonstrating how Landau quantization and magnetic confinement modify the stability of these three-body complexes. More recently, Ref. [282] addressed a central difficulty of the magnetotriion problem: the non-separability of *c.m.* and internal degrees of freedom. By applying a unitary transformation to the three-particle Schrödinger equation, the translational-internal entanglement was explicitly accounted for. Finally, Ref. [283] critically reassessed the two-dimensional trion problem, demonstrating that the exact inclusion of Coulomb-induced LL mixing is essential for reliable predictions of binding energies, which are otherwise significantly underestimated in high-field regimes.

The application of a perpendicular magnetic field introduces additional confinement and modifies both the kinetic energy and the internal structure of trions in 2D semiconductors. In the presence of a uniform magnetic field  $\mathbf{B} = B\hat{z}$ , the canonical momentum is replaced by the prescription  $\mathbf{p}_i \rightarrow \mathbf{p}_i - \frac{q_i}{c}\mathbf{A}(\mathbf{r}_i)$ , where  $q_i$  is the charge of the  $i$ th particle and  $\mathbf{A}$  is the vector potential, typically chosen in the symmetric gauge

$$\mathbf{A}(\mathbf{r}) = \frac{1}{2}\mathbf{B} \times \mathbf{r}. \quad (39)$$

For a trion,  $X^\pm$  in magnetic field, the Hamiltonian (3) becomes

$$\hat{H}_m = \sum_{i=1}^3 \frac{1}{2m_i} \left[ \mathbf{p}_i - \frac{q_i}{c} \mathbf{A}(\mathbf{r}_i) \right]^2 + \sum_{i<j} V(r_{ij}), \quad (40)$$

where  $V(r_{ij})$  is the screened Coulomb interaction.

In contrast to the zero-field case,  $B = 0$ , the *c.m.* and relative motions no longer fully decouple due to the magnetic vector potential. Therefore, the *c.m.* motion cannot be separated from the internal degrees of freedom in the conventional way. As shown in Ref. [49], the proper theoretical treatment of trions in a magnetic field must be based on magnetic translation symmetry rather than on naive separation of the *c.m.* motion. Because a trion carries net charge, ordinary translational invariance is broken, standard momentum conservation is replaced by magnetic translations, and the components of the magnetic translation operator become noncommuting.

The pseudomomentum operator was first introduced in the study of excitons in a magnetic field by Gor'kov and Dzyaloshinskii [284], where it was shown to commute with the exciton Hamiltonian and is therefore conserved. Following Refs. [285, 286], for  $X^\pm$  trions in a uniform perpendicular magnetic field, the conserved magnetic-translation (pseudomomentum) operator can be written as

$$\hat{\mathbf{K}} = \sum_{i=1}^3 \left[ \hat{\mathbf{p}}_i - \frac{q_i}{c} \mathbf{A}(\mathbf{r}_i) + \frac{q_i}{c} \mathbf{B} \times \mathbf{r}_i \right], \quad (41)$$

which satisfies  $[\hat{H}_m, \hat{\mathbf{K}}] = 0$ . However, for a charged trion with total charge  $Q = \sum_i q_i \neq 0$ , the components of  $\hat{\mathbf{K}}$  obey the noncommutative algebra

$$[\hat{K}_x, \hat{K}_y] = -i\hbar \frac{QB}{c}, \quad (42)$$

so that  $\hat{K}_x$  and  $\hat{K}_y$  do not commute, and so that  $\hat{K}_x$  and  $\hat{K}_y$  cannot be simultaneously diagonalized. Consequently, only  $\hat{\mathbf{K}}^2$  is conserved and is used to classify magnetotriion states. For  $Q \neq 0$ , this structure leads to Landau-like quantization of the trion *c.m.* motion and modifies the internal binding energy.

In Ref. [282], the trion is described by a three-particle Schrödinger equation with the magnetic field introduced through a vector potential in the symmetric gauge. Using coordinate and unitary transformations, the Hamiltonian is decomposed into: (i) a translational term describing Landau quantization of the *c.m.* motion, (ii) an internal binding term, and (iii) a translational–internal coupling term, linear in the magnetic-field strength, accounting for *c.m.*–internal entanglement.

The eigenenergies and wavefunctions are obtained variationally, with the trial wavefunction constructed as a linear combination of products of internal trion states and Landau-level functions, explicitly incorporating *c.m.*–internal mixing. The internal part is expanded in Slater-type orbitals, and each eigenstate is characterized by a shell number, spin permutation number, total angular momentum, and degeneracy index. Applied to hole-doped WSe<sub>2</sub> monolayers up to 25 T, the method predicts excited trion states stabilized and bound by a perpendicular magnetic field, explaining bright and dark triplet structures in magneto-optical spectra.

A more rigorous treatment was presented in Ref. [283], where two-dimensional magnetotriions were reexamined. It was shown that neglecting Coulomb-induced mixing between LLs leads to substantial underestimation of binding energies in experimentally relevant fields, and that this deficiency persists even at very high fields.

By treating Coulomb mixing exactly and preserving translational symmetry via magnetic translations, the full trion Hamiltonian was numerically diagonalized. Additional discrete states were identified; for example, in GaAs a second triplet state appears near  $B \approx 9$  T. Exact LL mixing also shifts the continuum boundary and increases binding energies (e.g., in a GaAs quantum well at 30 T, from 1.298 meV to 4.680 meV).

A central conceptual result of [283] is the demonstration that Coulomb-induced Landau-level mixing does not vanish even at high magnetic fields. Although Landau-level spacing increases linearly with  $B$ , the Coulomb matrix elements scale as  $\sqrt{B}$ , so second-order corrections remain finite in the strong-field limit. Also, the work further provides a comprehensive database of matrix elements for computing magnetotriion spectra in a wide range of materials.

Collectively, both studies [282, 283] demonstrate that a reliable description of magnetotriions requires an explicit treatment of the coupling between *c.m.* and internal degrees of freedom, and the exact inclusion of Coulomb-induced LL mixing, which are essential for reliable predictions of binding energies and discrete-state structure in quasi-two-dimensional systems.

Overall, these symmetry-consistent and Landau-level-complete approaches provide a rigorous framework for describing magnetotriions, highlighting the pivotal role of Coulomb-induced Landau-level mixing and *c.m.*–internal coupling in interpreting high-field experiments on 2D semiconductors.

## IX. CONCLUDING REMARKS

This review has traced the conceptual and methodological evolution of trion physics from its origins in bulk semiconductors to its modern realization in atomically thin materials. What began as an effective-mass analogue of the negative hydrogen ion has developed into a rich and quantitatively precise field of few-body physics in reduced dimensionality. The dramatic enhancement of Coulomb interactions in two-dimensional systems—driven by reduced dielectric screening and quantum confinement—has elevated trions from weakly bound excitonic complexes to robust quasiparticles with binding energies reaching tens or even hundreds of meV.

A central theme emerging from this review is the complementarity between few-body and many-body approaches. Deterministic variational methods, stochastic variational techniques, hyperspherical harmonics, Faddeev equations, and quantum Monte Carlo simulations now provide benchmark-level predictions for binding energies and structural properties of trions in two-dimensional semiconductors. At the same time, experimental progress—particularly in TMDC monolayers and anisotropic materials such as phosphorene—has confirmed the essential role of dielectric environment, effective-mass anisotropy, and carrier density in shaping trion spectra.

Several open directions define the outlook of the field. First, a unified theoretical description that consistently bridges few-body bound states and exciton–polaron regimes at finite doping remains an active challenge. Second, the treatment of trions in external magnetic fields requires fully symmetry-consistent, Landau-level–complete frameworks capable of handling strong Landau-level mixing and the nonseparability of center-of-mass and internal motion. Third, anisotropic and quasi-1D monolayers, including phosphorene and transition-metal trichalcogenides, offer promising platforms for exploring direction-dependent few-body correlations and dimensional crossover effects.

Equally important is the experimental frontier. High-quality, charge-tunable, and encapsulated devices are essential for resolving trion fine structure, intervalley configurations, and magnetotriton states in emerging material families such as Xenes and TMTCs. The continued interplay between advanced spectroscopy and rigorous few-body theory will be crucial for refining interaction models beyond simplified screening approximations.

In a broader perspective, trions provide a paradigmatic realization of few-body Coulomb physics embedded within a many-body solid-state environment. Their study not only deepens our understanding of correlated quasiparticles in low dimensions but also establishes a bridge between nuclear-style few-body methods and condensed-matter phenomena. As materials platforms expand and computational techniques continue to mature, trion physics is poised to remain a central arena for testing and advancing few-body concepts in quantum materials.

## ACKNOWLEDGMENTS

R. Ya. K. is grateful to K. Ziegler, A. Spiridonova, and Sh. M. Tsiklauri for valuable discussions.

- 
- [1] G. H. Wannier, The structure of electronic excitation levels in insulating crystals, *Phys. Rev.* **52**, 191 (1937).
  - [2] N. F. Mott, *Conduction in Non-Crystalline Materials*, Oxford University Press, Oxford (1968).
  - [3] F. Bassani and G. Pastori Parravicini, *Electronic States and Optical Transitions in Solids*, Pergamon Press, Oxford (1975).
  - [4] G. C. La Rocca, Wannier–Mott Excitons in Semiconductors, in *Thin Films and Nanostructures*, **31**, pp. 97–128, 2003, V. M. Agranovich and G. F. Bassani (eds.), Elsevier, San Diego (2003), Chap. 2.
  - [5] J. Knoester and V. M. Agranovich, Electronic excitations in organic solids, **31**, pp. 97–128, 2003, in *Thin Films and Nanostructures*, V. M. Agranovich and G. F. Bassani (eds.), Elsevier, San Diego (2003), Chap. 1.
  - [6] L. Lampert, Mobile and immobile effective-mass-particle complexes in nonmetallic solids, *Phys. Rev. Lett.* **1**, 450 (1958).
  - [7] S. A. Moskalenko, Recombination of excitons bound to impurities, *Fiz. Tverd. Tela* **2**, 139 (1960) [*Sov. Phys. Solid State* **2**, 155 (1960)].
  - [8] N. F. Mott, Excitons in semiconductors, *Adv. Phys.* **13**, 325 (1964).
  - [9] M. Taniguchi, M. Hirano, and S. Narita, Very shallow trapping state in doped germanium, *Phys. Rev. Lett.* **35**, 1095 (1975).
  - [10] S. Narita and M. Taniguchi, Uniaxial stress effect on the electron affinity of the  $D^-$  state in germanium, *Phys. Rev. Lett.* **36**, 913 (1976).
  - [11] M. Taniguchi and S. Narita,  $D^-$  state in silicon, *Solid State Commun.* **20**, 131 (1976).
  - [12] H. Kamimura, K. Taniguchi, and H. Sakaki, Negative donor ion states in semiconductors, *J. Phys. Chem. Solids* **40**, 907 (1979).
  - [13] Y.-C. Chang, Theory of negative donor ion states in semiconductors, *Phys. Rev. B* **25**, 3927 (1982).
  - [14] I. Filikhin, R. Ya. Kezerashvili, and B. Vlahovic, On binding energy of trions in bulk materials, *Phys. Lett. A* **382**, 787–791 (2018).
  - [15] D. M. Whittaker and A. J. Shields, Trions in semiconductor quantum wells, *Phys. Rev. B* **56**, 15185 (1997).

- [16] K. Kheng, R. T. Cox, Y. Merle d' Aubigné, F. Bassani, K. Saminadayar, and S. Tatarenko, Observation of negatively charged excitons  $X^-$  in semiconductor quantum wells, *Phys. Rev. Lett.* **71**, 1752 (1993).
- [17] G. Finkelstein, H. Shtrikman, and I. Bar-Joseph, Charged excitons in semiconductor quantum wells, *Phys. Rev. Lett.* **74**, 976 (1995).
- [18] A. J. Shields, J. L. Osborne, M. Y. Simmons, M. Pepper, and D. A. Ritchie, Charged excitons in GaAs quantum wells, *Phys. Rev. B* **52**, R5523 (1995).
- [19] H. Buhmann, L. Mansouri, J. Wang, P. H. Beton, N. Mori, L. Eaves, M. Henini, and M. Potemski, Magneto-optical studies of charged excitons in quantum wells, *Phys. Rev. B* **51**, 7969 (1995).
- [20] G. Finkelstein, H. Shtrikman, and I. Bar-Joseph, Charged excitons in GaAs-AlGaAs quantum wells, *Phys. Rev. B* **53**, R1709 (1996).
- [21] R. A. Suris and R. A. Sergeev, The  $X^-$  trion in a system with spatial separation of charge carriers, *Semiconductors* **37**, 1205 (2003).
- [22] W. Y. Ruan, K. S. Chan, H. P. Ho, R. Q. Zhang, and E. Y. B. Pun, Hyperspherical approach for charged excitons in quantum wells, *Phys. Rev. B* **60**, 5714 (1999).
- [23] L. C. O. Dacal and J. A. Brum, Binding energy of charged excitons in semiconductor quantum wells using configuration interaction, *Phys. Rev. B* **65**, 115324 (2002).
- [24] A. Wójs, Exact diagonalization studies of trion energy spectra in high magnetic fields, *Phys. Rev. B* **75**, 085318 (2007).
- [25] A. V. Filinov, C. Riva, F. M. Peeters, Yu. E. Lozovik, and M. Bonitz, Influence of well-width fluctuations on the binding energy of excitons, charged excitons, and biexcitons in GaAs-based quantum wells, *Phys. Rev. B* **70**, 035323 (2004).
- [26] C. Riva, F. M. Peeters, and K. Varga, Binding energies of excitonic complexes in quantum wells, *Phys. Rev. B* **61**, 13873 (2000).
- [27] A. Esser, E. Runge, R. Zimmermann, and Langbein *et al.*, Photoluminescence and radiative lifetime of trions in GaAs quantum wells, *Phys. Rev. B* **62**, 8232 (2000).
- [28] R. J. Warburton, C. S. Dürr, K. Karrai, J. P. Kotthaus, G. Medeiros-Ribeiro, and P. M. Petroff, Charged excitons in self-assembled quantum dots, *Phys. Rev. Lett.* **79**, 5282 (1997).
- [29] G. Finkelstein, V. Umansky, I. Bar-Joseph, V. Ciulin, S. Haacke, J.-D. Ganière, and B. Deveaud, Charged excitons in GaAs quantum wells: Optical properties and localization, *Phys. Rev. B* **58**, 12637 (1998).
- [30] V. Ciulin, P. Kossacki, S. Haacke, J.-D. Ganière, B. Deveaud, A. Esser, R. Zimmermann, and E. Runge, Localization effects on charged excitons in semiconductor quantum wells, *Phys. Rev. B* **62**, R16310 (2000).
- [31] A. Esser, R. Zimmermann, and E. Runge, Theory of charged excitons in semiconductor nanostructures, *Phys. Status Solidi A* **178**, 489 (2000).
- [32] A. Esser, R. Zimmermann, and E. Runge, Theory of trion spectra in semiconductor nanostructures *Phys. Status Solidi A* **227**, 317 (2001).
- [33] A. Esser, Y. Yayon, and I. Bar-Joseph, Charged excitons in disordered quantum wells, *Phys. Status Solidi A* **234**, 266 (2002).
- [34] T. Vanhoucke, M. Hayne, M. Henini, and V. V. Moshchalkov, Magneto-optical properties of charged excitons in GaAs quantum wells, *Phys. Rev. B* **65**, 041307 (2002).
- [35] G. V. Astakhov, D. R. Yakovlev, V. P. Kochereshko, W. Ossau, J. Cibert, A. Waag, and J. P. Reithmaier, Fine structure of charged excitons in semiconductor quantum wells, *Phys. Rev. B* **65**, 165335 (2002).
- [36] A. S. Bracker, E. A. Stinaff, D. Gammon, M. E. Ware, J. G. Tischler, A. Shabaev, A. L. Efros, and D. S. Katzer, Binding energies and recombination dynamics of charged excitons in quantum dots, *Phys. Rev. B* **72**, 035332 (2005).
- [37] R. A. Sergeev, R. A. Suris, G. V. Astakhov, W. Ossau, and D. R. Yakovlev, Charged excitons in semiconductor quantum wells with spatial separation of carriers, *Eur. Phys. J. B* **47**, 541 (2005).
- [38] G. V. Astakhov and W. Ossau, Charged excitons in semiconductor nanostructures, *Phys. Status Solidi C* **4**, 3310 (2007).
- [39] G. Munschy and B. Stébé, Charged excitons in semiconductors, *Phys. Status Solidi B* **64**, 213 (1974).
- [40] B. Stébé, Theory of charged excitons in semiconductors, *Nuovo Cimento B* **39**, 507 (1977).
- [41] B. Stébé, E. Feddi, and G. Munschy, Binding energies of charged excitons in semiconductors, *Phys. Rev. B* **35**, 4331 (1987).
- [42] B. Stébé and A. Ainane, Ground state energy and optical absorption of excitonic trions in two-dimensional semiconductors, *Superlatt. Microstruct.* **5**, 545 (1989).
- [43] A. Wójs and P. Hawrylak, Optical properties of charged excitons in semiconductor quantum dots, *Phys. Rev. B* **51**, 10880 (1995).
- [44] B. Stébé, G. Munschy, L. Stauffer, F. Dujardin, and J. Murat, Charged excitons in semiconductor quantum wells, *Phys. Rev. B* **56**, 12454 (1997).
- [45] J. Usukura, Y. Suzuki, and K. Varga, Few-body calculations of charged excitons in low-dimensional systems, *Phys. Rev. B* **59**, 5652 (1999).
- [46] B. Stébé and A. Moradi, Binding energies of charged excitons in semiconductor nanostructures, *Phys. Rev. B* **61**, 2888 (2000).
- [47] B. Stébé, A. Moradi, and F. Dujardin, Theoretical comparative study of negatively and positively charged excitons in GaAs/Ga<sub>1-x</sub>Al<sub>x</sub>As quantum wells, *Phys. Rev. B* **61**, 7231 (2000).
- [48] B. Szafran, B. Stébé, J. Adamowski, and S. Bednarek, Charged excitons in semiconductor quantum nanostructures, *J. Phys.: Condens. Matter* **12**, 2453 (2000).
- [49] A. B. Dzyubenko and A. B. Sivachenko, Magneto-optical spectroscopy of charged excitons, *Phys. Rev. Lett.* **84**, 4429 (2000).

- [50] F. M. Peeters, C. Riva, and K. Varga, Trions in quantum wells, *Physica B* **300**, 139 (2001).
- [51] I. Szlufarska, A. Wójs, and J. J. Quinn, Charged excitons in high magnetic fields, *Phys. Rev. B* **63**, 085305 (2001).
- [52] W. F. Xie, Binding energies of charged excitons in semiconductor nanostructures, *Phys. Status Solidi B* **226**, 247 (2001).
- [53] L. C. O. Dacal and J. A. Brum, Charged excitons in semiconductor quantum wells, *Phys. Rev. B* **65**, 115324 (2002).
- [54] Y. P. Varshni, Excitons and charged excitons in semiconductors, *Phys. Status Solidi B* **227**, 621 (2001).
- [55] L. C. O. Dacal, R. Ferreira, G. Bastard, and J. A. Brum, Excitonic complexes in low-dimensional semiconductor structures, *Phys. Rev. B* **65**, 115325 (2002).
- [56] B. Szafran, T. Chwiej, F. M. Peeters, S. Bednarek, J. Adamowski, and B. Partoens, Few-body states of charged excitons in semiconductor nanostructures, *Phys. Rev. B* **71**, 205316 (2005).
- [57] K. S. Novoselov, A. K. Geim, S. V. Morozov, D. Jiang, Y. Zhang, S. V. Dubonos, I. V. Grigorieva, and A. A. Firsov, Electric field effect in atomically thin carbon films, *Science* **306**, 666 (2004).
- [58] K. F. Mak, C. Lee, J. Hone, J. Shan, and T. F. Heinz, Atomically thin MoS<sub>2</sub>: A new direct-gap semiconductor, *Phys. Rev. Lett.* **105**, 136805 (2010).
- [59] S. Cahangirov, M. Topsakal, E. Aktürk, H. Şahin, and S. Ciraci, Two- and one-dimensional honeycomb structures of silicon and germanium, *Phys. Rev. Lett.* **102**, 236804 (2009).
- [60] Y. Xu, B. Yan, H.-J. Zhang, J. Wang, G. Xu, P. Tang, W. Duan, and S.-C. Zhang, Large-gap quantum spin Hall insulators in tin films, *Phys. Rev. Lett.* **111**, 136804 (2013).
- [61] B. Lalmi, H. Oughaddou, H. Enriquez, A. Kara, S. Vizzini, B. Ealet, and B. Aufray, Epitaxial growth of a silicene sheet, *Appl. Phys. Lett.* **97**, 223109 (2010).
- [62] P. Vogt, P. De Padova, C. Quaresima, J. Avila, E. Frantzeskakis, M. C. Asensio, A. Resta, B. Ealet, and G. Le Lay, Silicene: Compelling experimental evidence for graphene-like two-dimensional silicon, *Phys. Rev. Lett.* **108**, 155501 (2012).
- [63] M. E. Dávila, L. Xian, S. Cahangirov, A. Rubio, and G. Le Lay, Germanene: A novel two-dimensional germanium allotrope akin to graphene and silicene, *New J. Phys.* **16**, 095002 (2014).
- [64] F.-F. Zhu, W.-J. Chen, Y. Xu, C.-L. Gao, D.-D. Guan, C.-H. Liu, D. Qian, S.-C. Zhang, and J.-F. Jia, Epitaxial growth of two-dimensional stanene, *Nat. Mater.* **14**, 1020 (2015).
- [65] G. R. Bhimanapati, Z. Lin, V. Meunier, Y. Jung, J. Cha, S. Das, D. Xiao, Y. Son, M. S. Strano, V. R. Cooper et al., Recent advances in two-dimensional materials beyond graphene, *ACS Nano* **9**, 11509 (2015).
- [66] K. S. Novoselov, A. Mishchenko, A. Carvalho, and A. H. Castro Neto, 2D materials and van der Waals heterostructures, *Science* **353**, aac9439 (2016).
- [67] M. Velický and P. S. Toth, From two-dimensional materials to their heterostructures: An electrochemist's perspective, *Appl. Mater. Today* **8**, 68 (2017).
- [68] D. Jariwala, T. J. Marks, and M. C. Hersam, Mixed-dimensional van der Waals heterostructures, *Nat. Mater.* **16**, 170 (2017).
- [69] A. Kormányos, G. Burkard, M. Gmitra, J. Fabian, V. Zólyomi, N. D. Drummond, and V. Fal'ko,  $\mathbf{k}\cdot\mathbf{p}$  theory for two-dimensional transition metal dichalcogenide semiconductors, *2D Mater.* **2**, 022001 (2015).
- [70] J. O. Island, G. A. Steele, H. S. J. van der Zant, and A. Castellanos-Gomez, Environmental instability of few-layer black phosphorus, *2D Mater.* **2**, 011002 (2015).
- [71] Y. Li, A. Chernikov, X. Zhang, A. Rigosi, H. M. Hill, A. M. van der Zande, J. Hone, and T. F. Heinz, Measurement of the optical dielectric function of monolayer transition-metal dichalcogenides: MoS<sub>2</sub>, MoSe<sub>2</sub>, WS<sub>2</sub>, and WSe<sub>2</sub>, *Phys. Rev. B* **90**, 205422 (2014).
- [72] T. Cao, G. Wang, W. Han, H. Ye, C. Zhu, J. Shi, Q. Niu, P. Tan, E. Wang, B. Liu, and J. Feng, Valley-selective circular dichroism of monolayer molybdenum disulphide, *Nat. Commun.* **3**, 887 (2012).
- [73] F. Wang, A. Chernikov, and T. F. Heinz, Excitons in atomically thin transition metal dichalcogenides, *Nat. Photonics* **9**, 699 (2015).
- [74] L. Matthes, O. Pulci, and F. Bechstedt, Optical properties of two-dimensional honeycomb crystals graphene, silicene, germanene, and tinene from first principles, *Phys. Rev. B* **89**, 035438 (2014).
- [75] A. Molle, J. Goldberger, M. Houssa, Y. Xu, S. C. Zhang, and D. Akinwande, Buckled two-dimensional Xene sheets, *Nat. Mater.* **16**, 163 (2017).
- [76] G. Brunetti, C. Di Francesco, and G. Scamarcio, Tunable electronic and optical properties of Xenenes, *Phys. Rev. B* **97**, 035439 (2018).
- [77] V. I. Fal'ko and A. V. Shytov, Graphene and its analogues: Silicene, germanene, and beyond, *Phys. Rev. B* **86**, 035424 (2012).
- [78] M. E. Dávila, L. Xian, S. Cahangirov, A. Rubio, and G. Le Lay, Germanene: A novel two-dimensional germanium allotrope akin to graphene and silicene, *New J. Phys.* **16**, 095002 (2014).
- [79] Ff. Zhu, Wj. Chen, Y. Xu, *et al.*, Epitaxial growth of two-dimensional stanene, *Nat. Mater.* **14**, 1020 (2015).
- [80] A. J. Mannix, X.-F. Zhou, B. Kiraly, J. D. Wood, D. Alducin, B. D. Myers, X. Liu, B. L. Fisher, U. Santiago, J. R. Guest *et al.*, Synthesis of borophenes: Anisotropic, two-dimensional boron polymorphs, *Science* **350**, 1513 (2015).
- [81] R. Ya. Kezerashvili, Trions in three-, two- and one-dimensional materials, in *Recent Progress in Few-Body Physics*, edited by N. Orr, M. Płoszajczak, F. Marqués, and J. Carbonell, Springer Proceedings in Physics **238** (Springer, Cham, 2020), pp. 827–831.
- [82] N. S. Rytova, Screened potential of a point charge in a thin film, *Proc. MSU, Phys., Astron.* **3**, 30 (1967).
- [83] L. V. Keldysh, Coulomb interaction in thin semiconductor and semimetal films, *JETP Lett.* **29**, 658 (1979) [*Zh. Eksp. Teor. Fiz. Pis' ma Red.* **29**, 716 (1979)].

- [84] P. Cudazzo, C. Attaccalite, I. V. Tokatly, and A. Rubio, Dielectric screening in two-dimensional insulators: Implications for excitonic and impurity states, *Phys. Rev. B* **84**, 085406 (2011).
- [85] D. V. Tuan, M. Yang, and H. Dery, Coulomb interaction in monolayer transition-metal dichalcogenides, *Phys. Rev. B* **98**, 125308 (2018).
- [86] M. Zinkiewicz, M. Grzeszczyk, L. Kipczak, et al., The effect of dielectric environment on the brightening of neutral and charged dark excitons in WSe<sub>2</sub> monolayer. *Appl. Phys. Lett.* **120**, 163101 (2022).
- [87] A. Kratzer, Die ultraroten Rotationspektren der Halogenwasserstoffe, *Z. Phys.* **3**, 289 (1920).
- [88] M. R. Molas, A. Slobodeniuk, K. Nogajewski, M. Bartosiak, D. Basko, and M. Potemski, Energy spectrum of two-dimensional excitons in a nonuniform dielectric medium, *Phys. Rev. Lett.* **123**, 136801 (2019).
- [89] R. Ya. Kezerashvili, J. Luo, and C. R. Malvino, On an exactly solvable two-body problem in two-dimensional quantum mechanics with Kratzer-type potentials, *Few Body Syst.* **64**, 79 (2023).
- [90] T. G. Pedersen, Stark effect in nonhydrogenic low-dimensional excitons, *Phys. Rev. B* **107**, 195419 (2023).
- [91] R. Ya. Kezerashvili, J. Luo, C. R. Malvino, and A. Spiridonova, Kratzer and Modified Kratzer Potentials in Two Dimensions: Exact Solutions and Exciton Applications, *Int. J. Theor. Phys.* **64**, 278 (2025).
- [92] K. F. Mak, K. He, C. Lee, G. H. Lee, J. Hone, T. F. Heinz, and J. Shan, Tightly bound trions in monolayer MoS<sub>2</sub>, *Nature Materials* **12**, 207 (2013).
- [93] J. S. Ross, S. Wu, H. Yu, et al., Electrical control of neutral and charged excitons in a monolayer semiconductor, *Nature Communications* **4**, 1474 (2013).
- [94] B. Zhu, X. Chen, and X. Cui, Exciton binding energy of monolayer WS<sub>2</sub>, *Scientific Rep.* **5**, 9218 (2015).
- [95] J. Jadczyk, J. Kutrowska-Girzycka, et al., Probing of free and localized excitons and trions in atomically thin WS<sub>2</sub>, *Nano Lett.* **17**, 7057 (2017).
- [96] Y. Chen, S. Li, et al., Positive and negative trions in monolayer WSe<sub>2</sub> under electrostatic doping, *Phys. Rev. B* **107**, 045412 (2023).
- [97] J. Huang, T. He, et al., Exciton and trion dynamics in monolayer WSe<sub>2</sub>, *Scientific Rep.* **6**, 22414 (2016).
- [98] J. Yang, T. Lu, et al., Optical tuning of exciton and trion emissions in monolayer MoTe<sub>2</sub>, *ACS Nano* **9**, 6603 (2015).
- [99] S. Biswas, M. Baranowski, et al., Rydberg excitons and trions in monolayer MoTe<sub>2</sub>, arXiv:2302.03720 (2023). <https://authors.library.caltech.edu/records/1xgfh-w8557>
- [100] A. T. Hanbicki *et al.*, Large range modification of exciton species in monolayer WS<sub>2</sub>, *Appl. Opt.* **55**, 6251 (2016).
- [101] J. W. Christopher *et al.*, Temperature-dependent photoluminescence of trions in monolayer MoS<sub>2</sub>, *Sci. Rep.* **7**, 14062 (2017).
- [102] D. A. Nguyen *et al.*, Temperature dependence of exciton and trion states in monolayer WSe<sub>2</sub>, *Sci. Rep.* **14**, 64303 (2024).
- [103] D. K. Efimkin and A. H. MacDonald, Many-body theory of trion absorption features in 2D semiconductors, *Phys. Rev. B* **95**, 035417 (2017).
- [104] M. Sidler *et al.*, Fermi polaron–polaritons in charge-tunable atomically thin semiconductors, *Nat. Phys.* **13**, 255 (2017).
- [105] Y. Lin, X. Ling, S. Yu, et al., Dielectric screening of excitons and trions in single-layer MoS<sub>2</sub>, *Nano Lett.* **14**, 5569 (2014).
- [106] G. Plechinger, P. Nagler, A. Arora, R. Schmidt, A. Chernikov, et al., Trion fine structure and coupled spin–valley dynamics in monolayer tungsten disulfide, *Nat. Commun.* **7**, 12715 (2016).
- [107] Y. Zhang, H. Li, H. Wang, R. Liu, S. Zhang, and Z. Qiu, On valence-band splitting in layered MoS<sub>2</sub>. *ACS Nano* **9**, 8514 (2015).
- [108] A. M. Jones, H. Yu, N. J. Ghimire, et al., Optical generation of excitonic valley coherence in monolayer WSe<sub>2</sub>. *Nat. Nanotechnol.* **8**, 634 (2013).
- [109] G. Wang, L. Bouet, D. Lagarde, et al., Valley dynamics probed through charged and neutral exciton emission in monolayer WSe<sub>2</sub>. *Phys. Rev. B* **90**, 075413 (2014).
- [110] A. Singh, G. Moody, S. Wu, et al., Coherent electronic coupling in atomically thin MoSe<sub>2</sub>. *Phys. Rev. Lett.* **112**, 21680 (2014).
- [111] C. H. Lui, A. J. Frenzel, D. V. Pilon, et al., Trion-induced negative photoconductivity in monolayer MoS<sub>2</sub>. *Phys. Rev. Lett.* **113**, 166801 (2014).
- [112] C. Zhang, H. Wang, W. Chan, C. Manolatos, and R. Rana, Absorption of light by excitons and trions in monolayers of metal dichalcogenide MoS<sub>2</sub>: Experiments and theory *Phys. Rev. B* **89**, 205436 (2014).
- [113] B. Zhu, H. Zeng, J. Dai, Z. Gong, and X. Cui, Anomalously robust valley polarization and valley coherence in bilayer WS<sub>2</sub>. *Proc. Natl. Acad. Sci. U.S.A.* **111**, 11606 (2014).
- [114] J. Yang, T. Lü, Y. W. Myint, J. Pei, D. Macdonald, J. Zheng, and Y. Lu, Robust excitons and trions in monolayer MoTe<sub>2</sub>. *ACS Nano* **9**, 6603 (2015).
- [115] J. Shang, X. Shen, C. Cong, N. Peimyoo, B. Cao, M. Eginligil, and T. Yu, Observation of excitonic fine structure in a 2D transition-metal dichalcogenide semiconductor. *ACS Nano* **9**, 647 (2015).
- [116] G. Plechinger, P. Nagler, J. Kraus, N. Paradiso, C. Strunk, C. Schüller, and T. Korn, Identification of excitons, trions and biexcitons in single-layer WS<sub>2</sub>. *Phys. Status Solidi RRL* **9**, 457 (2015).
- [117] A. Singh, G. Moody, K. Tran, et al., Trion formation dynamics in monolayer transition metal dichalcogenides, *Phys. Rev. B* **93**, 041401(R) (2016).
- [118] M. Drüppel, T. Deilmann, P. Krüger, and M. Röhlfing, Diversity of trion states and substrate effects in the optical properties of an MoS<sub>2</sub> monolayer. *Nat. Commun.* **8**(1), 2117 (2017).
- [119] E. Courtade, M. Semina, M. Manca, et al., Charged excitons in monolayer WSe<sub>2</sub>: experiment and theory. *Phys. Rev. B* **96**, 085302 (2017).

- [120] F. Volmer, S. Pissinger, M. Ersfeld, S. Kuhlen, C. Stampfer, and B. Beschoten, Intervalley dark trion states with spin lifetimes of 150 ns in WSe<sub>2</sub>. *Phys. Rev. B* **95**, 235408 (2017).
- [121] E. Liu, J. van Baren, Z. Lu, et al., Gate tunable dark trions in monolayer WSe<sub>2</sub>. *Phys. Rev. Lett.* **123**, 027401 (2019).
- [122] S. Borghardt and B. E. Kardynał, Interplay of excitonic complexes in p-doped WSe<sub>2</sub> monolayers. *Phys. Rev. B* **101**, 161402(R) (2020).
- [123] J. Klein, M. Florian, A. Hotger, et al., Trions in MoS<sub>2</sub> of intra- and intervalley spin states. *Phys. Rev. B* **105**, L041302 (2022).
- [124] K-Q. Lin, et al., High-lying valley-polarized trions in 2D semiconductors. *Nat. Comm.* **13**, 6980 (2022).
- [125] C. Hou, J. Deng, J. Guan, et al., Photoluminescence of monolayer MoS<sub>2</sub>, modulated by water/O<sub>2</sub>/laser irradiation, *Phys. Chem. Chem. Phys.* **23**, 24579 (2021).
- [126] J. Yang, R. Xu, J. Pei, Y. Myint, F. Wang, Z. Wang, S. Zhang, Y. Yu, L. Wang, and Y. Zhao, Optical tuning of exciton and trion emissions in monolayer phosphorene, *Light: Science & Applications* **4**, e312 (2015).
- [127] R. Xu, S. Zhang, F. Wang, J. Yang, Z. Wang, J. Pei, Y. W. Myint, B. Xing, Z. Yu, L. Fu, Q. Qin, and Y. Lu, Extraordinarily Bound Quasi-One-Dimensional Trions in Two-Dimensional Phosphorene Atomic Semiconductors, *ACS Nano* **10**, 2046 (2016).
- [128] J. Yang and Y. Lu, Optical properties of phosphorene, *Chin. Phys. B* **26**, 034201 (2017).
- [129] S. Yoon, T. Kim, S.-Y. Seo, S.-H. Shin, S.-B. Song, B. J. Kim, et al., Electrical control of anisotropic and tightly bound excitons in bilayer phosphorene, *Phys. Rev. B* **103**, L041407 (2021).
- [130] M. R. Molas, L. Macewicz, A. Wieloszyńska, et al., Photoluminescence as a probe of trions and excitons in black phosphorus, *npj 2D Mater Appl* **5**, 83 (2021).
- [131] A. Surrente, A. A. Mitioglu, K. Galkowski, W. Tabis, D. K. Maude, and P. Plochocka, Excitons in atomically thin black phosphorus, *Phys. Rev. B* **93**, 121405(R) (2016).
- [132] P. Liang, D. Cao, and X. Chen, Refined dielectric screening and many-body effects on trion binding energies in anisotropic phosphorene, *Phys. Chem. Chem. Phys.* **26**, 11825 (2024).
- [133] W. Sheng, Many-body theory of trions in two-dimensional nanostructures, *Appl. Phys. A* **130**, 885 (2024).
- [134] Y. Jin, X. Li, and J. Yang, Single layer of MX<sub>3</sub> (M = Ti, Zr; X = S, Se, Te): A new platform for nano-electronics and optics, *Phys. Chem. Chem. Phys.* **17**, 18665 (2015).
- [135] M. Li, J. Dai, and X. C. Zeng, Tuning the electronic properties of transition-metal trichalcogenides via tensile strain, *Nanoscale* **7**, 15385 (2015).
- [136] J. Dai, M. Li, and X. C. Zeng, Group IVB transition metal trichalcogenides: A new class of 2D layered materials beyond graphene, *WIREs Comput. Mol. Sci.* **6**, 211 (2016).
- [137] A. Patra and C. Rout, Anisotropic quasi-one-dimensional layered transition-metal trichalcogenides: Synthesis, properties, and applications, *RSC Adv.* **10**, 36413 (2020).
- [138] M. Chen, L. Li, M. Xu, W. Li, L. Zheng, and X. Wang, Quasi-one-dimensional van der Waals transition metal trichalcogenides, *Research (Wash. D.C.)* **6**, 0066 (2023).
- [139] E. Torun, H. Sahin, A. Chaves, L. Wirtz, and F. M. Peeters, Ab initio and semiempirical modeling of excitons and trions in monolayer TiS<sub>3</sub>, *Phys. Rev. B* **98**, 075419 (2018).
- [140] J. Zhao, A. Buldum, J. Han, and J. P. Lu, Rise of silicene: A competitive 2D material, *Prog. Mater. Sci.* **83**, 24 (2016).
- [141] E. Scalise, M. Houssa, G. Pourtois, V. V. Afanas'ev, and A. Stesmans, Silicene on non-metallic substrates: Recent theoretical and experimental advances, *Nano Res.* **11**, 1163 (2018).
- [142] M. W. Ochapski and D. Kaczorowski, Progress in epitaxial growth of stanene, *Open Phys.* **20**, 251 (2022).
- [143] R. Ya. Kezerashvili, Sh. M. Tsiklauri, and A. Spiridonova, Controllable trions in buckled two-dimensional materials, *Phys. Rev. B* **110**, 035425 (2024).
- [144] R. Ya. Kezerashvili, Sh. M. Tsiklauri, and A. Spiridonova, Electric-field-tuned binding energies of trions in silicene, germanene, and stanene monolayers, *Int. J. Phys.* **12**, 225 (2024).
- [145] E. Cinquanta *et al.*, Dynamics of Two Distinct Exciton Populations in Methyl-Functionalized Germanene, *Nano Lett.* **22**, 1153 (2022).
- [146] I. Kupchak, F. Bechstedt, O. Pulci *et al.*, Tuning the optical absorption and exciton bound states of functionalized germanene, *Sci. Rep.* **14**, 25182 (2024).
- [147] M. N. Brunetti, O. L. Berman, and R. Ya. Kezerashvili, Optical properties of excitons in buckled two-dimensional materials in an external electric field, *Phys. Rev. B* **98**, 125406 (2018).
- [148] R. Ya. Kezerashvili and A. Spiridonova, Effects of parallel electric and magnetic fields on Rydberg excitons in buckled two-dimensional materials, *Phys. Rev. B* **103**, 165410 (2021).
- [149] N. W. Ashcroft and N. D. Mermin, *Solid State Physics* (Holt, Rinehart and Winston, New York, 1976).
- [150] P. Y. Yu and M. Cardona, *Fundamentals of Semiconductors: Physics and Materials Properties* (Springer, Berlin, 2010).
- [151] D. Xiao, G. B. Liu, W. Feng, X. Xu, and W. Yao, Coupled spin and valley physics in monolayers of MoS<sub>2</sub> and other group-VI dichalcogenides, *Phys. Rev. Lett.* **108**, 196802 (2012).
- [152] S. Manzeli, D. Ovchinnikov, D. Pasquier, O. V. Yazyev, and A. Kis, 2D transition metal dichalcogenides, *Nat. Rev. Mater.* **2**, 17033 (2017).
- [153] E. Mostaani, M. Szyniszewski, C. H. Price, R. Maezono, M. Danovich, R. J. Hunt, N. D. Drummond, and V. I. Fal'ko, Diffusion quantum Monte Carlo study of excitonic complexes in two-dimensional transition-metal dichalcogenides, *Phys. Rev. B* **96**, 075431 (2017).
- [154] R. Tempelaar and T. C. Berkelbach, Many-body simulation of two-dimensional electronic spectroscopy of excitons and trions in monolayer transition metal dichalcogenides, *Nature Communications*, **10**(1), 3419 (2019).

- [155] M. Van der Donck, M. Zarenia, and F. M. Peeters, Excitons and trions in monolayer transition metal dichalcogenides: a comparative study between the multiband model and the quadratic single-band model. *Phys. Rev. B* **96**, 035131 (2017).
- [156] T. C. Berkelbach, M. S. Hybertsen, and D. R. Reichman, Theory of neutral and charged excitons in monolayer transition metal dichalcogenides, *Phys. Rev. B* **88**, 045318 (2013).
- [157] Y.-W. Chang and Y.-C. Chang, Variationally optimized orbital approach to trions in two-dimensional materials, *J. Chem. Phys.* **155**, 024110 (2021).
- [158] S. Wu, L. Cheng, and Q. Wang, Exciton states and absorption spectra in freestanding monolayer transition metal dichalcogenides: A variationally optimized diagonalization method, *Phys. Rev. B* **100**, 115430 (2019).
- [159] M. A. Semina and R. A. Suris, Localized excitons and trions in semiconductor nanosystems, *Phys. Usp.* **65** (2), 111–130 (2022).
- [160] Y. Suzuki and K. Varga, *Stochastic Variational Approach to Quantum-Mechanical Few-Body Problems* (Springer, New York, 1998).
- [161] J. Mitroy, S. Bubin, W. Horiuchi, Y. Suzuki, L. Adamowicz, W. Cencek, K. Szalewicz, J. Komasa, D. Blume, and K. Varga, Theory and application of explicitly correlated Gaussians, *Rev. Mod. Phys.* **85**, 693–749 (2013).
- [162] D. W. Kidd, D. K. Zhang, and K. Varga, Binding energies and structures of two-dimensional excitonic complexes in transition metal dichalcogenides, *Phys. Rev. B* **93**, 125423 (2016).
- [163] J. Yan and K. Varga, Excited-state trions in two-dimensional materials. *Phys. Rev. B* **101**, 235435 (2020).
- [164] D. K. Zhang, D. W. Kidd, and K. Varga, Excited biexcitons in transition metal dichalcogenides, *Nano Lett.* **15**, 7002 (2015).
- [165] C. Fey, P. Schmelcher, A. Imamoğlu, and R. Schmidt, Theory of exciton–electron scattering and trion formation in two-dimensional materials, *Phys. Rev. B* **101**, 195417 (2020).
- [166] S. S. Kumar, B. C. Mulkerin, A. Tiene, F. M. Marchetti, M. M. Parish, and J. Levinsen, Efficient calculation of trion energies in monolayer transition metal dichalcogenides, *Phys. Rev. B* **111**, 085404 (2025).
- [167] E. Hiyama, M. Kamimura, T. Motoba, T. Yamada, and Y. Yamamoto, Three-body structure of hypernuclei studied with the Gaussian expansion method, *Phys. Rev. Lett.* **85**, 270 (2000).
- [168] H. Kamada, M. Kamimura, Y. Fukushima, and K. Miyagawa, Benchmark test calculation of the four-nucleon bound state, *Phys. Rev. C* **64**, 044001 (2001).
- [169] E. Hiyama, Y. Kino, and M. Kamimura, Gaussian expansion method for few-body systems, *Prog. Part. Nucl. Phys.* **51**, 223–307 (2003).
- [170] E. Hiyama, B. F. Gibson, and M. Kamimura, Four-body cluster structure of hypernuclei, *Phys. Rev. C* **70**, 031001 (2004).
- [171] E. Hiyama, M. Kamimura, Y. Yamamoto, and T. Motoba, Five-body cluster structure of double- $\Lambda$  hypernucleus  ${}_{\Lambda\Lambda}^{11}\text{Be}$ , *Phys. Rev. Lett.* **104**, 212502 (2010).
- [172] E. Hiyama and M. Kamimura, Variational calculation of few-body systems using the Gaussian expansion method, *Phys. Rev. A* **85**, 022502 (2012).
- [173] L. G. M. Tenório, A. J. Chaves, E. Hiyama, and T. Frederico, Gaussian expansion method for few-body states in two-dimensional materials, arXiv:2602.11386 [cond-mat.mes-hall] (2026). :contentReference[oaicite:0]index=0
- [174] B. L. Hammond, W. A. Lester, and P. J. Reynolds, *Monte Carlo Methods in Ab Initio Quantum Chemistry* (World Scientific, Singapore, 1994).
- [175] W. M. C. Foulkes, L. Mitas, R. J. Needs, and G. Rajagopal, Quantum Monte Carlo simulations of solids, *Rev. Mod. Phys.* **73**, 33 (2001).
- [176] D. M. Ceperley and B. J. Alder, Ground state of the electron gas by a stochastic method, *Phys. Rev. Lett.* **45**, 566 (1980).
- [177] M. Troyer and U.-J. Wiese, Computational Complexity and Fundamental Limitations to Fermionic Quantum Monte Carlo Simulations, *Phys. Rev. Lett.* **94**, 110201 (2005).
- [178] J. Glimm and A. Jaffe, *Quantum Physics: A Functional Integral Point of View*, 2nd ed. (Springer-Verlag, New York, 1987).
- [179] J. W. Negele and H. Orland, *Quantum Many-Particle Systems* (Addison-Wesley, Reading, MA, 1988).
- [180] D. M. Ceperley, Path integrals in the theory of condensed helium, *Rev. Mod. Phys.* **67**, 279 (1995).
- [181] M. Z. Mayers, T. C. Berkelbach, M. S. Hybertsen, and D. R. Reichman, Binding energies and spatial structures of small carrier complexes in monolayer transition metal dichalcogenides via diffusion Monte Carlo, *Phys. Rev. B* **92**, 161404(R) (2015).
- [182] M. Szyniszewski, E. Mostaani, N. D. Drummond, and V. I. Fal’ko, Binding energies of trions and biexcitons in two-dimensional semiconductors from diffusion quantum Monte Carlo calculations, *Phys. Rev. B* **95**, 081301(R) (2017).
- [183] E. Mostaani, M. Szyniszewski, N. D. Drummond, and V. I. Fal’ko, Diffusion quantum Monte Carlo study of excitonic complexes in two-dimensional transition-metal dichalcogenides, *Phys. Rev. B* **96**, 075431 (2017).
- [184] E. Mostaani, N. D. Drummond, M. Szyniszewski, and V. I. Fal’ko, Charge-carrier complexes in monolayer semiconductors, *Phys. Rev. B* **108**, 035420 (2023).
- [185] R. P. Feynman, Space-time approach to non-relativistic quantum mechanics, *Rev. Mod. Phys.* **20**, 367 (1948).
- [186] R. P. Feynman and A. R. Hibbs, *Quantum Mechanics and Path Integrals* (McGraw-Hill, New York, 1965).
- [187] H. F. Trotter, On the product of semi-groups of operators, *Proc. Amer. Math. Soc.* **10**, 545 (1959).
- [188] M. Suzuki, Generalized Trotter’s formula and systematic approximants of exponential operators and inner derivations with applications to many-body problems, *Commun. Math. Phys.* **51**, 183 (1976).
- [189] V. S. Filinov, V. E. Fortov, M. Bonitz, and Zh. Moldabekov, Fermionic path integral Monte Carlo results for the uniform electron gas at finite temperature. *Phys. Rev. E* **91**, 033108 (2015).

- [190] I. Kylänpää and H.-P. Komsa, Binding energies of exciton complexes in transition metal dichalcogenide monolayers and effect of dielectric environment, *Phys. Rev. B* **92**, 205418 (2015).
- [191] K. A. Velizhanin and A. Saxena, Excitonic effects in two-dimensional semiconductors: Path-integral Monte Carlo study, *Phys. Rev. B* **92**, 195305 (2015).
- [192] A. V. Filinov, M. Bonitz, and Yu. E. Lozovik, First-principles approach to binding energies of excitons, trions and biexcitons in quantum wells, *Phys. Status Solidi C* **0**(5), 1441 (2003).
- [193] A. V. Filinov, M. Bonitz, and Yu. E. Lozovik, Excitonic clusters in coupled quantum dots, *J. Phys. A: Math. Gen.* **36**, 5899–5904 (2003).
- [194] S. Weiss and M. Bonitz, Path-integral Monte Carlo simulations for interacting few-electron quantum dots with spin-orbit coupling, *Phys. Rev. B* **72**, 245301 (2005).
- [195] A. Filinov, M. Bonitz, and K. Varga, Spectrum of excitonic complexes in monolayers of transition-metal dichalcogenides, *Phys. Rev. A* **95**, 032510 (2017).
- [196] O. Witham, R. J. Hunt, and N. D. Drummond, Stability of trions in coupled quantum wells modelled by two-dimensional bilayers, *Phys. Rev. B* **97**, 075424 (2018).
- [197] L. D. Faddeev, Scattering theory for a three-particle system. *ZhETF* **39**, 1459 (1961); [*Sov. Phys. JETP* **12**, 1014 (1961)].
- [198] L. D. Faddeev, Mathematical problems of the quantum theory of scattering for a system of three particles. *Proc. Math. Inst. Acad. Sciences USSR* **69**, 1 (1963).
- [199] S.P. Merkuriev, C. Gignoux, and A. Laverne, Three-body scattering in configuration space, *Ann. Phys. (N.Y.)* **99**, 30 (1976).
- [200] L.D. Faddeev and S.P. Merkuriev, *Quantum Scattering Theory for Several Particle Systems* (Kluwer Academic, Dordrecht, 1993) pp. 398.
- [201] I. Filikhin, R. Ya. Kezerashvili, Sh. M. Tsiklauri, and B. Vlahovic, Trions in bulk and monolayer materials: Faddeev equations and hyperspherical harmonics, *Nanotechnology* **29**, 124002 (2018).
- [202] K. Mohseni, M. R. Hadizadeh, T. Frederico, D. R. da Costa, and A. J. Chaves, Trion clustering structure and binding energy in two-dimensional semiconductor materials: Faddeev equations approach, *Phys. Rev. B* **107**, 165427 (2023).
- [203] R. Ya. Kezerashvili, Sh. M. Tsiklauri, I. Filikhin, V. M. Suslov, and B. Vlahovic, Three-body calculations for the  $K^-pp$  system within potential models. *J. Phys. G: Nucl. Part. Phys.* **43**, 065104 (2016).
- [204] I. Filikhin, R. Ya. Kezerashvili, V. M. Suslov, Sh. M. Tsiklauri, and B. Vlahovic, Three-body model for  $K(1460)$  resonance. *Phys. Rev. D* **102**, 094027 (2020).
- [205] I. Filikhin, R. Ya. Kezerashvili, and B. Vlahovic, The charge and mass symmetry breaking in the  $KK\bar{K}$  system. *J. Phys. G: Nucl. Part. Phys.* **51**, 035102 (2024).
- [206] I. Filikhin, R. Ya. Kezerashvili, and B. Vlahovic, Possible  ${}^3_\phi\text{H}$  hypernucleus with HAL QCD interaction. *Phys. Rev. D* **110**, L031502 (2024).
- [207] I. Filikhin, R. Ya. Kezerashvili, and B. Vlahovic, Study of light  $\phi$ -mesic nuclei with HAL QCD  $\phi N$  interactions, *J. Subatomic Particles & Cosmology*, **4**, 100117 (2025).
- [208] I. Filikhin, R. Ya. Kezerashvili, and B. Vlahovic, Examination of the lattice QCD-motivated strong attractive  $\Omega N$  potentials in the  $\Omega^-np$  system, *Phys. Rev. D* **111**, 114518 (2025).
- [209] W. Ruan, K. S. Chan, and E. Y. B. Pun, Application of hyperspherical coordinates to two-dimensional charged excitons, *J. Phys.: Condens. Matter* **12**, 7905 (2000).
- [210] R. Ya. Kezerashvili, L. L. Margolin, and Sh. M. Tsiklauri, Three-electron quantum dot in a magnetic field, *Few-Body Syst.* **44**, 241–244 (2008).
- [211] W. Xie, The negatively charged exciton in double-layer quantum dots, *Eur. Phys. J. B* **17**, 385–389 (2000).
- [212] W.-F. Xie, Charged-Exciton Complexes in Quantum Dots, *Phys. Status Solidi B* **226**, 247 (2001).
- [213] R. I. Jibuti and K. V. Shitikova, *Method of Hyperspherical Functions in Atomic and Nuclear Physics* (Energoatomizdat, Moscow, 1993) (in Russian).
- [214] J. Avery, *Hyperspherical Harmonics: Applications in Quantum Theory* (Kluwer Academic Publishers, Dordrecht, 1989).
- [215] J. E. Avery and J. S. Avery, *Hyperspherical Harmonics and Their Applications* (World Scientific, London, 2018).
- [216] C. G. Bao, Charged-exciton complexes in quantum dots, *Chin. Phys. Lett.* **20**, 1665 (2003).
- [217] R. Ya. Kezerashvili and Sh. M. Tsiklauri, Biexciton and triexciton states in quantum dots, *Few-Body Syst.* **54**, 1653–1657 (2013).
- [218] R. Ya. Kezerashvili and Sh. M. Tsiklauri, Trion and Biexciton in Monolayer Transition Metal Dichalcogenides, *Few-Body Syst.* **58** (2017).
- [219] R. Ya. Kezerashvili, Sh. M. Tsiklauri, and A. Dublin, Trions in two-dimensional monolayers within the hyperspherical harmonics method: Application to transition metal dichalcogenides, *Phys. Rev. B* **109**, 085406 (2024).
- [220] R. Ya. Kezerashvili, *Few-Body Systems in Condensed Matter Physics*. *Few-Body Syst.* **60**, 52 (2019).
- [221] M. Braun and S. A. Vugalter, Three-particle bound states in two-dimensional systems, *Phys. Rev. B* **50**, 16688 (1994).
- [222] M. Braun and S. A. Vugalter, Exciton complexes in two-dimensional semiconductors, *Phys. Rev. B* **51**, 17207 (1995).
- [223] K. F. Mak, K. He, J. Shan, and T. F. Heinz, Control of valley polarization in monolayer  $\text{MoS}_2$  by optical helicity. *Nat. Nanotechnol.* **7**, 494 (2012).
- [224] H. Zeng, J. Dai, W. Yao, D. Xiao, and X. Cui, Valley polarization in  $\text{MoS}_2$  monolayers by optical pumping, *Nat. Nanotechnol.* **7**, 490 (2012).
- [225] G. Sallen, L. Bouet, X. Marie, G. Wang, C. R. Zhu, W. P. Han, Y. Lu, P. H. Tan, T. Amand, B. L. Liu et al., *Phys. Rev. B* **86**, 081301 (2012).

- [226] G. Wang, E. Palleau, T. Amand, S. Tongay, X. Marie, and B. Urbaszek, Polarization and time-resolved photoluminescence spectroscopy of excitons in MoSe<sub>2</sub> monolayers. *Appl. Phys. Lett.* **106**, 112101 (2015).
- [227] D. MacNeill, C. Heikes, K.-F. Mak, et al., Breaking of valley degeneracy by magnetic field in monolayer MoSe<sub>2</sub>. *Phys. Rev. Lett.* **114**, 037401 (2015).
- [228] F. Gao, Y. Gong, M. Titze, et al., Valley trion dynamics in monolayer MoSe<sub>2</sub>. *Phys. Rev. B* **94**, 245413 (2016).
- [229] T. Yan, J. Ye, X. Qiao, P. Tan, and X. Zhanga, Exciton valley dynamics in monolayer WSe<sub>2</sub> probed by the two-color ultrafast Kerr rotation. *Phys. Chem. Chem Phys.* **4**, 2599 (2017).
- [230] J. Huang, T. B. Hoang, T. Ming, J. Kong, and M. H. Mikkelsen. Temporal and spatial valley dynamics in two-dimensional semiconductors probed via Kerr rotation. *Phys. Rev. B* **95**, 075428 (2017).
- [231] K. Hao et al., Trion valley coherence in monolayer semiconductors. *2D Mater.* **4**, 025105 (2017).
- [232] H. Yu, X. Cui, X. Xu, and W. Yao, Valley excitons in two-dimensional semiconductors. *Natl. Science Rev.* **2**, 57 (2015).
- [233] B. Ganchev, N. Drummond, I. Aleiner, and V. Fal'ko, Three-particle complexes in two-dimensional semiconductors. *Phys. Rev. Lett.* **114**, 107401 (2015).
- [234] J. Fu, J. M. R. Cruz, and F. Qu, Valley dynamics of different trion species in monolayer WSe<sub>2</sub>. *Appl. Phys. Lett.* **115**, 082101 (2019).
- [235] X.-X. Zhang, T. Cao, Z. Lu, Y.-C. Lin, F. Zhang, Y. Wang, et al., Magnetic brightening and control of dark excitons in monolayer WSe<sub>2</sub>. *Nat. Nanotechnol.* **12**, 883 (2017).
- [236] C. Robert, T. Amand, F. Cadiz, D. Lagarde, E. Courtade, M. Manca, T. Taniguchi, K. Watanabe, B. Urbaszek, and X. Marie, Fine structure and lifetime of dark excitons in transition metal dichalcogenide monolayers, *Phys. Rev. B* **96**, 155423 (2017).
- [237] X. Xu, W. Yao, D. Xiao, and T. F. Heinz, Spin and pseudospins in layered transition metal dichalcogenides, *Nat. Phys.* **10**, 343 (2014).
- [238] G. Wang, A. Chernikov, M. M. Glazov, T. F. Heinz, X. Marie, T. Amand, and B. Urbaszek, Colloquium: Excitons in atomically thin transition metal dichalcogenides, *Rev. Mod. Phys.* **90**, 021001 (2018).
- [239] Z. Li, T. Wang, Z. Lu, C. Jin, Y. Chen, Y. Meng, et al., Revealing the biexciton and trion-exciton complexes in BN encapsulated WSe<sub>2</sub>. *Nat. Commun.* **9**, 3719 (2018).
- [240] A. Torche and G. Bester, First-principles many-body theory for charged and neutral excitations: Trion fine structure splitting in transition metal dichalcogenides. *Phys. Rev. B* **100**, 201403(R) (2019).
- [241] T. Deilmann and K. S. Thygesen, Dark excitations in monolayer transition metal dichalcogenides. *Phys. Rev. B* **96**, 201113(R) (2017).
- [242] M. Danovich, V. Zolyomi, and V. I. Fal'ko, Dark trions and biexcitons in WS<sub>2</sub> and WSe<sub>2</sub> made bright by e-e scattering. *Sci. Rep.* **7**, 45998 (2017).
- [243] T. C. Berkelbach and D. R. Reichman, Optical and excitonic properties of atomically thin transition-metal dichalcogenides, *Annu. Rev. Condens. Matter Phys.* 2018. **9**, 379–96 (2018).
- [244] M. V. Durnev and M. M. Glazov, Excitons and trions in two-dimensional semiconductors based on transition metal dichalcogenides, *Phys.-Usp.* **61**, 825 (2018).
- [245] M. A. Semina and R. A. Suris, Localized excitons and trions in semiconductor nanosystems. *Phys.-Usp.* **65**, 111 (2022).
- [246] F. Marsusi, E. Mostaani, and N. D. Drummond, Quantum Monte Carlo study of three-dimensional Coulomb complexes: Trions and biexcitons, hydrogen molecules and ions, helium hydride cations, and positronic and muonic complexes. *Phys. Rev. A* **106**, 062822 (2022).
- [247] M. Donck, M. Zarenia, and F. Peeters, Excitons, trions, and biexcitons in transition-metal dichalcogenides: Magnetic-field dependence, *Phys. Rev. B* **97**, 195408 (2018).
- [248] A. Ramirez-Torres, V. Turkowski, and T. S. Rahman, Time-dependent density-matrix functional theory for trion excitations: Application to monolayer MoS<sub>2</sub> and other transition-metal dichalcogenides. *Phys. Rev. B* **90**, 085419 (2014).
- [249] Y. V. Zhumagulov, A. Vagov, D. R. Gulevich, P. E. Faria Junior, and V. Perebeinos, Trion induced photoluminescence of a doped MoS<sub>2</sub> monolayer. *J. Chem. Phys.* **153**, 044132 (2020).
- [250] Y. V. Zhumagulov, A. Vagov, N. Yu. Senkevich, D. R. Gulevich, and V. Perebeinos, Three-particle states and brightening of intervalley excitons in a doped MoS<sub>2</sub> monolayer. *Phys. Rev. B* **101**, 245433 (2020).
- and trions in monolayer transition metal dichalcogenides: a comparative study between the multiband model and the quadratic single-band model. *Phys. Rev. B* **96**, 035131 (2017).
- [251] A. Arora, T. Deilmann, T. Reichenauer, J. Kern, et al., Excited-state trions in monolayer WS<sub>2</sub>. *Phys. Rev. Lett.* **123** 16, 167401 (2019).
- [252] M. Florian, M. Hartmann, A. Steinhoff, et al., The dielectric impact of layer distances on exciton and trion binding energies in van der waals heterostructures. *Nano Lett.* **18**, 2725 (2018).
- [253] J. Zipfel, K. Wagner, J. D. Ziegler, T. Taniguchi, K. Watanabe, M. A. Semina, and A. Chernikov, Light-matter coupling and non-equilibrium dynamics of exchange-split trions in monolayer WS<sub>2</sub>. *J. Chem. Phys.* **153**. 034706. 10.1063/5.0012721 (2020).
- [254] M. Glazov, Optical properties of charged excitons in two-dimensional semiconductors. *J. Chem. Phys.* **153**, 034703 (2020).
- [255] Y.-C. Chang, S.-Y. Shiau, and M. Combescot, Crossover from trion-hole complex to exciton-polaron in doped two-dimensional semiconductors, *Phys. Rev. B* **98**, 235203 (2018).
- [256] Y.-C. Chang and D. R. Reichman, Many-body theory of exciton-electron interactions in two-dimensional semiconductors, *Phys. Rev. B* **99**, 125421 (2019).
- [257] F. Rana, M. Koksai, and C. Manolatu, Many-body theory of the optical conductivity of two-dimensional semiconductors including excitons and trions, *Phys. Rev. B* **102**, 085304 (2020).

- [258] M. A. Semina, J. V. Mamedov, and M. M. Glazov, Excitons and trions with negative effective masses in two-dimensional semiconductors. *Oxford Open Materials Science*, **3**, itad004 (2023).
- [259] K. P. O'Donnell and X. Chen, Temperature dependence of semiconductor band gaps, *Appl. Phys. Lett.* **58**, 2924 (1991).
- [260] D. V. Tuan, A. M. Jones, M. Yang, X. Xu, and H. Dery, Virtual trions in the photoluminescence of monolayer transition-metal dichalcogenides. *Phys. Rev. Lett.*, **122**, 217401 (2019).
- [261] L. S. R. Cavalcante, D. R. da Costa, G. A. Farias, D. R. Reichman, and A. Chaves, Stark shift of excitons and trions in two-dimensional materials, *Phys. Rev. B* **98**, 245309 (2018).
- [262] A. Chaves, T. Low, P. Avouris, and F. M. Peeters, Theoretical investigation of electron-hole complexes in anisotropic two-dimensional materials, *Phys. Rev. B* **93**, 115314 (2016).
- [263] T. Deilmann and K. S. Thygesen, Unraveling the not-so-large trion binding energy in monolayer black phosphorus, *2D Mater.* **5**, 041007 (2018).
- [264] H. Zhong, J. Sheng, and Q. Wang, Electric-field-induced enhancement of excitonic binding in one-dimensional phosphorene nanostructures, *Phys. Chem. Chem. Phys.* **26**, 11204 (2024).
- [265] M. Chen, Y. Li, Y. Wang, J. Lin, and Y. Zhang, Quasi-one-dimensional van der Waals transition metal trichalcogenides, *Adv. Mater.* **35**, 2203651 (2023).
- [266] J. S. Ross, S. Wu, H. Yu, et al., Electrical control of neutral and charged excitons in a monolayer semiconductor, *Nat. Commun.* **4**, 1474 (2013).
- [267] E. Liu, J. van Baren, Z. Lu, et al., Gate tunable dark trions in monolayer WSe<sub>2</sub>, *Phys. Rev. Lett.* **123**, 027401 (2019).
- [268] R. Perea-Causin, S. Brem, F. Buchner, et al., Electrically tunable layer-hybridized trions in doped WSe<sub>2</sub> bilayers, *Nat. Commun.* **15**, 6713 (2024).
- [269] C. J. Tabert and E. J. Nicol, Dynamical polarization function, plasmons, and screening in silicene and other buckled honeycomb lattices, *Phys. Rev. B* **89**, 195410 (2014).
- [270] A. Srivastava, M. Sidler, A. V. Allain, D. S. Lembke, A. Kis, and A. Imamoglu, Valley Zeeman effect in elementary optical excitations in monolayer WSe<sub>2</sub>, *Nat. Phys.*, **11**(2):141 (2015).
- [271] G. Aivazian, Z. Gong, A. M. Jones, et al., Magnetic control of valley pseudospin in monolayer WSe<sub>2</sub>, *Nat. Phys.* **11**, 148 (2015).
- [272] A. A. Mitioglu, P. Plochocka, P. Kossacki, et al., Optical investigation of monolayer and bulk tungsten diselenide (WSe<sub>2</sub>) in high magnetic fields, *Nano Lett.* **15**, 4387 (2015).
- [273] T. P. Lyons, S. Dufferwiel, M. Brooks, et al., The valley Zeeman effect in inter- and intravalley trions in monolayer WSe<sub>2</sub>, *Nat. Commun.* **10**, 2330 (2019).
- [274] E. Liu, J. van Baren, Z. Lu, et al., Gate tunable dark trions in monolayer WSe<sub>2</sub>, *Phys. Rev. Lett.* **123**, 027401 (2019).
- [275] V. A. Kuznetsov, L. V. Kulik, M. A. Zudov, A. S. Zhuravlev, A. V. Khaetskii, I. V. Kukushkin, and J. L. Reno, Three-particle electron-hole complexes in two-dimensional electron systems, *Phys. Rev. B*, **98**:205303, 2018.
- [276] P. Kapuściński, D. Vaclavkova, M. Grzeszczyk, A. O. Slobodeniuk, K. Nogajewski, M. Bartoš, et al., Valley polarization of singlet and triplet trions in a WS<sub>2</sub> monolayer in magnetic fields, *Phys. Chem. Chem. Phys.* **22**, 19155–19161 (2020).
- [277] C. Riva, F. M. Peeters, and K. Varga, Magnetic field dependence of the energy of negatively charged excitons in semiconductor quantum wells, *Phys. Rev. B* **63**, 115302 (2001).
- [278] C. Riva, F. M. Peeters, and K. Varga, Positively charged magnetoexcitons in a semiconductor quantum well, *Phys. Rev. B* **64**, 235301 (2001).
- [279] T. Deilmann, P. Krüger, and M. Rohlfing, Ab initio studies of exciton  $g$  factors: Monolayer transition metal dichalcogenides in magnetic fields, *Phys. Rev. Lett.* **124**, 226402 (2020).
- [280] R. A. Sergeev, R. A. Suris, G. V. Astakhov, W. Ossau, and D. R. Yakovlev, Universal estimation of  $X^-$  trion binding energy in semiconductor quantum wells, *Eur. Phys. J. B* **47**, 41 (2005).
- [281] A. Wójs and J. J. Quinn, Exact-diagonalization studies of trion energy spectra in high magnetic fields, *Phys. Rev. B* **75**, 085318 (2007).
- [282] Y.-W. Chang and Y.-C. Chang, Trions in two-dimensional materials in a perpendicular magnetic field, *J. Chem. Phys.* **157**, 044104 (2022).
- [283] I. A. Aleksandrov, Two-dimensional trion in a magnetic field revisited, *Phys. Rev. B* **109**, 035307 (2024).
- [284] L. P. Gor'kov and I. E. Dzyaloshinskii, Contribution to the theory of the Mott exciton in a strong magnetic field, *Zh. Eksp. Teor. Fiz.* **53**, 717 (1967) [*Sov. Phys. JETP* **26**, 449 (1968)].
- [285] A. B. Dzyubenko, Two-dimensional charged electron-hole complexes in magnetic fields: Keeping magnetic translations preserved, *Solid State Commun.* **113**, 683 (2000).
- [286] A. B. Dzyubenko, Charged hydrogenic problem in a magnetic field: Noncommutative translations, unitary transformations, and coherent states, *Phys. Rev. B* **65**, 035318 (2001).